HERON is jointly edited by:
STEVIN-LABORATORY of the faculty of Civil Engineering, Delft University of Technology, Delft, The Netherlands
and
TNO BUILDING AND CONSTRUCTION RESEARCH. Rijswijk (ZH), The Netherlands
HERON contains contributions based mainly on research work performed in these laboratories on strength of materials, structures and materials science.

ISSN 0046-7316

Secretary:
J. G. M. van Mier
Stevinweg 1
P.O. Box 5048
2600 GA Delft, The Netherlands
Tel. 0031-15-784578
Fax 0031-15-611465
Telex 38151 BUTUD

HERON vol. 36 1991 no. 1

Contents

LATERALLY LOADED SINGLE PILE IN SOFT SOIL

J. L. Bijnagte
Delft Geotechnics

P. van den Berg
Delft Geotechnics

N. F. Zorn
Trischler und Partner GmbH
Formerly: Delft Geotechnics

H. A. Dieterman
Department of Civil Engineering,
Mechanics & Structures Division
Delft University of Technology

Publications in HERON since 1970

Laterally loaded single pile in soft soil - theory and reality -

1 Introduction

The possibility of verifying results of numerical calculations with full scale measurements is one of the most challenging tasks for research and design engineers. If the problem involves a continuum and interaction between soil and a structural member, additional aspects of interest are: how many dimensions should be taken into account, which aspects have to be modelled and which ones can be neglected? Determination of the soil properties is another problem that needs attention. Which tests have to be performed, and in what way should the tests results be transformed to model parameters?

In the context of a research project "Behaviour of Dolphins under Horizontal Loading", commissioned by the Dutch Ministry of Public Works (Rijkswaterstaat), Delft Geotechnics was put in a position in which a real benchmark problem could be presented: "The Analysis of a Single Pile in Soft Soil under Horizontal Loading". A group of engineers involved in numerical modelling at the Faculty of Civil Engineering of Delft University of Technology, from both the Section Geotechnics and the Mechanics & Structures Division were invited to participate. The project was initiated by Rijkswaterstaat because maintenance of dolphins shows that damage often occurs at locations where dolphins are placed in soils with weak top layers. On such locations the impact forces are higher than predicted. Apparently, the common design philosophy which ignores the contribution of the soft layers is not conservative for dynamic loads; it fails to model these circumstances correctly.

The project focussed on the analysis of 3-dimensional (3-D) soil resistance effects on a horizontally loaded single pile resembling a dolphin. Special attention was given to the contribution of soft top layers to the total soil resistance. To further increase the value of the results, both the influence of the calculation method and the soil investigations were included in the project.

In order to verify calculated results a full scale field test was included. An open steel pile was used for this test, on a location belonging to the Department of Wind Energy of Delft University. After the test this pile was used as single pile foundation for a windmill.

Soil conditions at the test location were characteristic for the Dutch canal system: soft soil layers on top of sand. The necessary soil investigations were performed at the test location and in Delft Geotechnics' laboratory.

Each party used their calculation model currently under development: Mechanics & Structures Division a 1-dimensional discrete element model, the Section Geotechnics a quasi 3-D model and Delft Geotechnics a full 3-D finite element model and, as a reference case, a commonly used 1-dimensional design model.

This publication presents the results of the joint project, including the modelling background necessary to understand the approaches used and the test results, which may serve as a reference case for the calibration of further models.

2 Project definition

The aim of the project was to gain further insight into the mechanisms that govern the behaviour of a single pile under horizontal loading, so that currently used design models, e.g. Matlock (1970) and Sullivan et al. (1980), could be reassessed for Dutch soil conditions. If necessary modifications could be drafted, or a new design model could be derived.

The problem that is analysed can further be subdivided into soil mechanical aspects, as for instance the determination of mechanical soil properties and applicable constitutive laws, and numerical modelling aspects, as for instance how many dimensions must be included and how the behaviour at the pile-soil interface can be simulated.

The different models used for the benchmark project are:

- a 1-dimensional, 1-D, discrete element model used by the Mechanics & Structures Division;
- a quasi 3-dimensional, q3-D, finite element model used by the Section Geotechnics
- a 3-dimensional, 3-D, finite element model used by Delft Geotechnics, and
- a commonly used Dutch design method, based on a 1-dimensional finite element model; these calculations were performed by Delft Geotechnics

An overview of the project on flow chart is presented in Fig. 2.1.

The project started with soil investigations:

level 1: cone penetration testing (CPT);

level 2: an undisturbed "Delft Continuous Sampler" boring, including laboratory analyses on the soil samples: soil classification tests, simple shear and triaxial testing;

level 3: pressuremeter testing, to determine stiffness and strength parameters of the soil in situ.

Each participant was requested to document very closely the procedure followed in deriving mechanical properties used in the calculations, and to submit the analysis results prior to receiving the next set of soil investigation results. The predictions can therefore be regarded as "class A" predictions. The information obtained from the previous soil investigation level(s) could also be used for the subsequent calculation.

Due to external complications the 3-D finite element calculations had to be performed after the test. The input however was fully documented before performing the field test, so curve-fitting to the test result was not possible. The results of all the predictions were compiled in a report and evaluated.

The full scale, horizontally loaded, pile test was performed on a previously installed hollow steel pile with a diameter of 0.61 m, a wall thickness of 8.8 mm and a length of 12.5 m. The pile was instrumented with 40 strain gauges distributed in the axial direction in 4 rows at 0°, 90°, 180° and 270° positions. Each row contained 10 gauges.

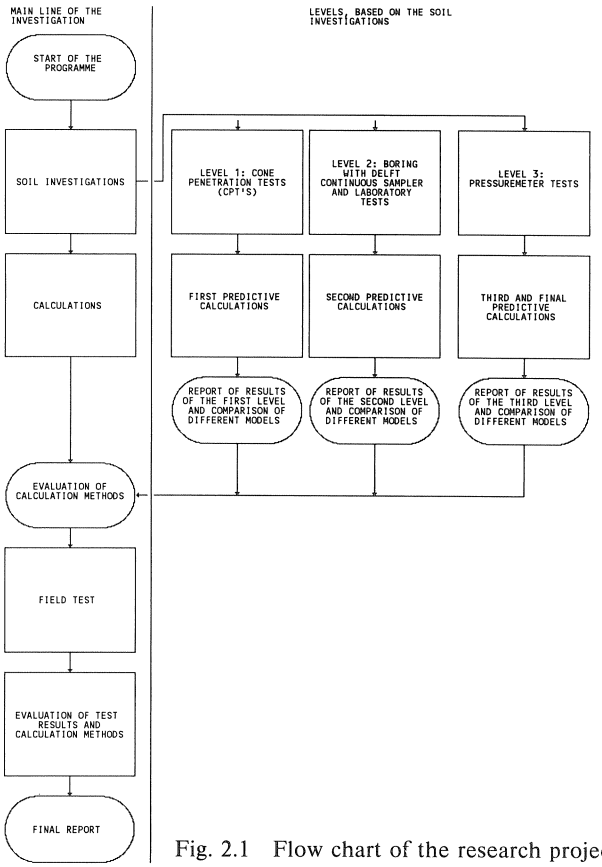

Fig. 2.1 Flow chart of the research project.

The strain gauges were protected against destruction during pile driving by steel U-profiles welded to the pile surface. The non circular cross-section of the pile is presented in Fig. 2.2.

The pile was located in layered soil with a groundwater table at 0.5 m below the surface. The soil consisted of a 0.5 m soil fill layer of silty sand (this layer was removed before the test), a 2 m thick clay layer, 0.5 m of peat and 4 m of clay above medium dense sand. The soil conditions can therefore be described as soft soil above sandy layers, simulating the soil conditions of Dutch dolphins quite well.

The test consisted of first a quasi-static horizontal loading, limited by a maximum measured pile strain of 0.1 %, second sine shaped, one-sided, loading cycles with loading periods of 9 s at about 60 and 75 % of the initial load level and last a quasi-static load to determine the degradation effect. The project was basically limited to the initial load-deflection behaviour and bending moment distribution. However, where possible, the cyclic behaviour, the behaviour of the pile-soil interface and soil strength degradation were also included in the calculations.

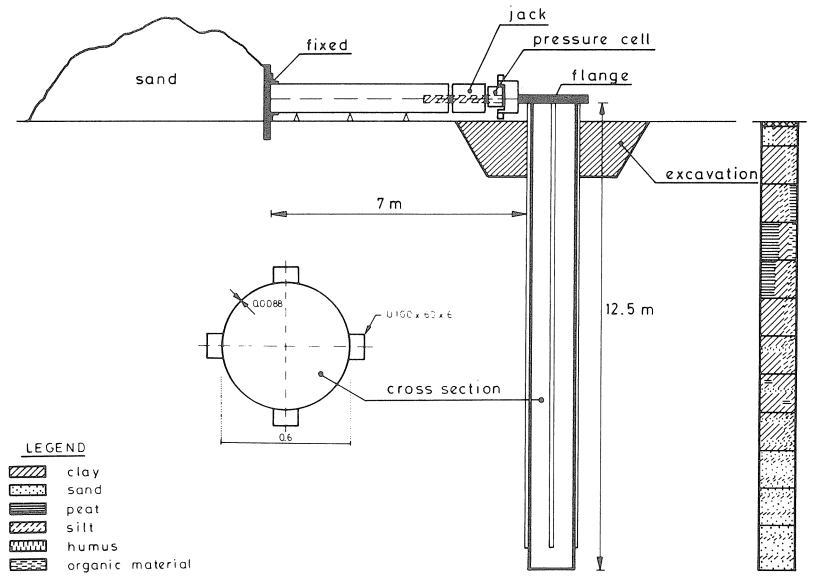

Fig. 2.2 Test pile.

The final step of the project is formed by the evaluation of the predictions and the comparison with the test results. This includes the mechanical reasoning that may help explain the differences between the predictions and their deviations from the test results.
Based on all the knowledge gained by the project, recommendations for future design and research were derived (Bijnagte and Berg, van den, 1989b).

3 Soil investigations

3.1 *Introduction*

An essential basis of the calculations are the mechanical properties of the soil in which the pile is placed. In order to derive these mechanical properties soil investigations are necessary. The extent may vary from minimal field investigations and rules of thumb to sophisticated in situ and laboratory investigations. In design analyses a rather rough estimation of the soil properties is often sufficient. Since the interpretation of a measured soil mechanical value to derive mechanical input values for a calculation method forms an important part of the benchmark project, information on the stiffness and strength parameters must in this case be as accurate as possible.
In order to investigate the contribution of additional soil investigations to the quality of a prediction three levels of soil investigation were selected for the benchmark calculations:

level 1: cone penetration testing (CPT);
level 2: boring with undisturbed sampling and laboratory tests;
level 3: pressuremeter tests.

These three levels of soil investigation will be introduced, and the results of the investigations discussed hereafter.

3.2 *Level 1: Cone penetration testing (CPT)*

Basically, cone penetration testing is the measurement of the soil resistance during the penetration of a cone with a projected area of 1000 mm^2 in the soil, at a penetration rate of 20 mm per second. Over time, the measurements have been extended to include also "local sleeve friction", pore-water pressures and the penetration angle. This allows a more accurate classification of the tested soil since the ratio of the local sleeve friction and the cone resistance can be related to the soil type, De Ruiter (1982). The excess pore-water pressures, generated by the cone penetration, are a measure of the permeability of the soil and can therefore also be related to the soil type.
Three CPT's were performed around the test pile, to a depth of 15 m from ground level. In all cases cone resistance, local sleeve friction and penetration angle were recorded, whereas pore-water pressures were recorded for CPT 01A. All CPT results show a good correlation and can be represented by CPT 01A, the diagram of which is shown in Fig. 3.1.

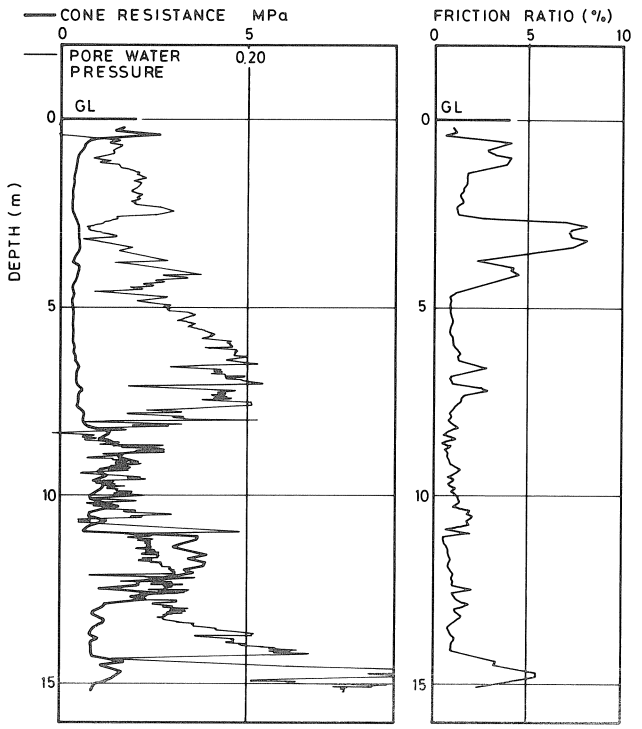

Fig. 3.1 CPT 01A: Registered cone resistance, local sleeve friction and pore-water pressures at the test site.

A more detailed description of the equipment and test procedure is given by De Ruiter (1982).

3.3 *Level 2: Boring and laboratory tests*

During this soil investigation level a boring was performed using the "Delft Continuous Sampler", diameter 66 mm, to a depth of 14 m from ground level.
The "Delft Continuous Sampler" allows the extraction of a continuous soil column at a test location. The sampler is pushed into the soil using standard CPT hydraulic jacks. The thrust is applied to heavy outer extension tubes, each 1 m long. The soil sample enters a specially manufactured impervious nylon stocking which is fed into plastic inner tubes that are also 1 m long each. A special drilling mud, which fills the space between the stocking and the plastic tube, is added to the sampler. The two main purposes of adding this mud are: lubrication, to minimize friction as the sample passes through the tubes, and lateral support of the sample, to prevent it from bulging. The unit weight of the mud is therefore designed to be similar to that of the soil.
Once the final penetration depth is reached the sampler is pulled up. On first pulling upwards, sampling retaining clamps are activated and prevent the sample from dropping downwards. The inner tubes containing the soil are cut into sections of 1 m length for ease of handling. A more detailed description of the equipment and sampling procedure is given by Begemann (1966).
The continuous sample taken at the test location was used for classification and determination of the density of the soil per m length of the sample. The results of the soil classification and wet densities are presented in Table 3.1 as a function of the sample depth.
Following these initial classifications, soil mechanical tests were performed on the samples taken from the boring:

Table 3.1 Soil classification and wet densities

depth in m – ground level	soil type	ϱ_{wet} (ton/m^3)
0.0 – 0.15	pavement	–
0.15 – 0.66	sand/clay, silty	1.88
0.66 – 1.67	clay, silty/clay, silty, with humus	1.58
1.67 – 2.68	clay, silty, with humus/peat	1.46
2.68 – 3.69	peat/clay, silty, with humus	1.06
3.69 – 4.70	peat/clay, silty	1.38
4.70 – 5.71	clay, silty	1.60
5.71 – 6.73	clay, silty, with humus/peat layer	1.40
6.73 – 7.75	clay, silty, with peat and a single layer of sand	1.42
7.75 – 8.77	clay, silty, with sand layers/sand	1.75
8.77 – 9.79	sand, with silt layers	1.69
9.79 – 10.81	sand, with silt- and clay layers	1.71
10.81 – 11.83	sand, with silt- and some clay layers	1.74
11.83 – 12.85	sand, with silt- and clay layers	1.74
12.85 – 13.85	sand, with silt layers/silt with sand layers	1.71

- density and water content determinations (10x);
- particle size distribution curve (5x);
- Atterberg liquid and plastic limit determination (6x);
- laboratory vane tests (8x);
- simple shear test (1x);
- triaxial tests (CU) (2x).

These tests are necessary to obtain more data about the physical and mechanical properties of the soil. Density, water content determination and sieve analysis (determination of the particle size distribution curve) are necessary for a more detailed soil mechanical classification. The Atterberg limits are used for the identification of the in situ conditions concerning the plastic range of the soil. Simple stress analysis is possible with the torsional shear tests; the laboratory vane tests. The simple shear test is used to determine the strength of soil under controlled stress conditions, while triaxial tests characterize soil behaviour under simulated in situ conditions.

The results of the water content determinations and the laboratory vane tests are shown in Table 3.2.

A particle size distribution curve of the sand present at the test site is shown in Fig. 3.2.

Table 3.2 Results of water content determinations and laboratory vane tests

Sample nr.	depth of the sample in m - ground level	soil type	wet density (ton/m^3)	water content (weight %)	undrained shear strength (c_u) (kN/m^2)
2	1.16 - 1.20	clay silty	1.53	72.5	36.2
3	2.07 - 2.11	clay silty with humus	1.62	58.9	17.2
4	2.98 - 3.02	peat	1.02	522.0	34.8
5	4.39 - 4.43	clay silty	1.70	48.3	9.9
6	5.27 - 5.31	clay silty	1.58	62.0	16.8
7A	6.21 - 6.25	clay silty with humus	1.40	109.6	26.9
7B	6.51 - 6.56	clay with peat	1.19	210.9	-
8A	7.10 - 7.15	peat with clay	1.13	251.6	-
8B	7.48 - 7.52	clay with humus	1.52	73.7	21.0
9	8.25 - 8.29	clay- and sand layers	1.65	54.5	6.8

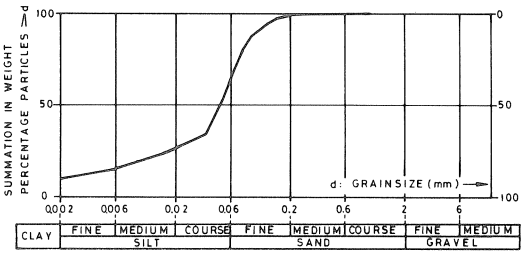

Fig. 3.2 Particle size distribution curve of sand from 8.25–8.35 m - ground level.

The results of the Atterberg limit tests are presented in Table 3.3. The liquid limit and plastic limit are defined as the watercontents determining the upper and lower bound of the plastic state of the soil. The plasticity index is defined as the liquid limit minus the plastic limit.

Table 3.3 Results of Atterberg limit tests for clay and peat samples

Sample nr.	depth of the sample in m - ground level	soil type	liquid limit (%)	plastic limit (%)	plasticity index (%)
2	1.16 - 1.26	clay silty	77.2	22.3	54.9
3	2.07 - 2.17	clay silty with humus	71.8	23.5	48.3
4	2.98 - 3.08	peat	631.0	234.4	396.6
5	4.39 - 4.49	clay silty	43.0	18.1	24.9
6	5.30 - 5.40	clay silty	59.2	18.7	40.5
7A	6.20 - 6.30	clay silty with humus	121.1	28.0	93.1

Peat is usually a very anisotropic material consisting of many more or less horizontally deposited layers being the remains of decomposed plants. The mechanical properties therefore strongly depend upon the direction of loading. In the direction of the layers, slip between the layers can take place relative easy. In the direction perpendicular to the layers however, the plant "fibres" have to be broken before large displacements can occur. It is therefore very important that the mechanical properties are established in a test that simulates both the size and the relative direction of the in situ loading. This is possible using the simple shear test. In this test the peat sample is placed in a box that consists of two halves. A so-called consolidation pressure is applied to simulate the in situ soil pressure. The two halves of the box are then given a relative horizontal movement, thus generating shear stresses in the soil sample.
The test can be performed using either constant pressure or by changing the vertical pressure in such a way that the volume of the soil is kept at a constant value during the test. Strictly speaking a constant volume test does not have to be undrained, however test results have shown that the difference is usually negligible.
Therefore, a "constant volume" simple shear test using a GEONOR apparatus, see Bjerrum and Landva (1966), was performed on a peat sample from a depth between 3.00 m - and 3.20 m - ground level. Consolidation of this sample took place at a vertical pressure of 21 kPa being the effective in situ vertical soil pressure.
The results of the test are presented in Fig. 3.3.
The triaxial test is widely used to determine the stiffness and strength characteristics of soil. A cylindrical soil sample sealed with a rubber membrane is placed in a pressurised chamber. The isotropic pressure in the chamber subjects the sample to equal stresses in three perpendicular directions. With a piston, a vertical load can be applied to the top of the sample. This increases the vertical pressure while the horizontal pressures remain constant. The increase in vertical loading is continued until the soil fails in shear, or large displacements have occurred. The vertical deformation, volume change and pore-

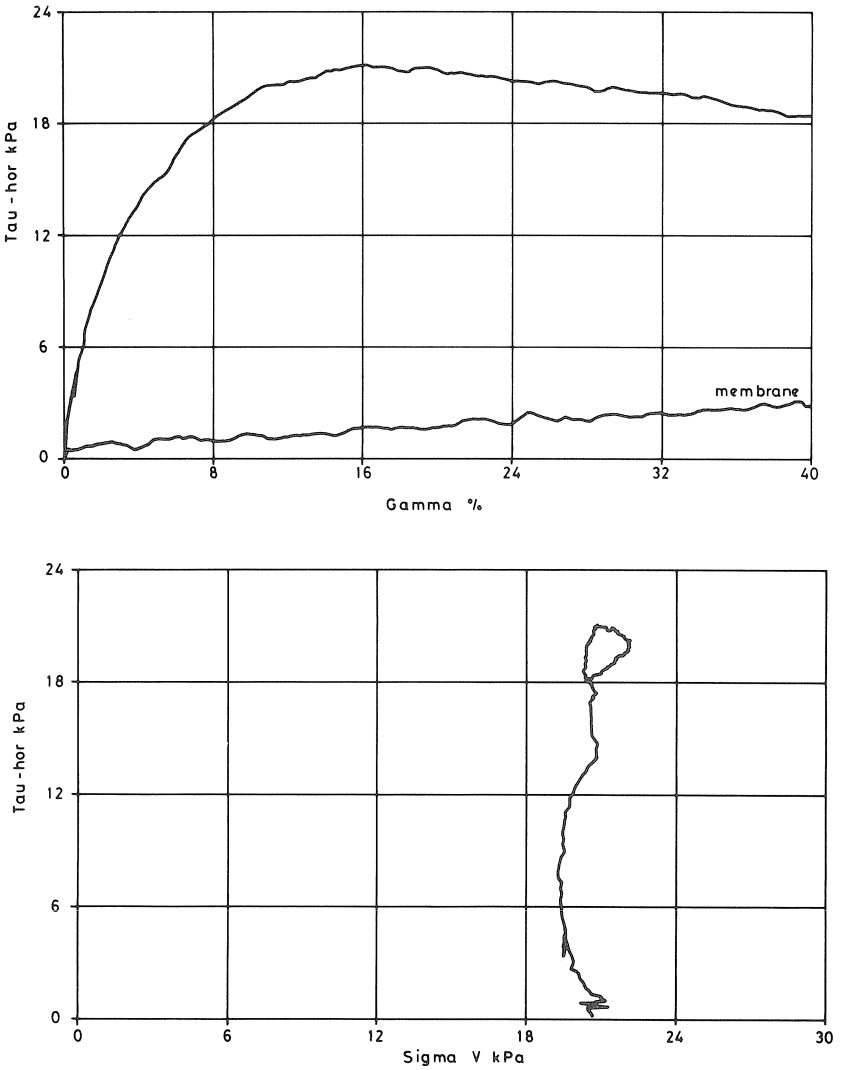

Fig. 3.3 Simple shear test results of a peat sample from a depth of 3.00–3.20 m – ground level: shear stress as a function of the shear strain (a) and shear stress as a function of the vertical stress (b).

water pressures can be recorded, and drainage conditions can be influenced. To obtain data of the soil strength under different horizontal stress levels it is best to perform separate tests at different stress levels. Sometimes, when there is only a small soil sample available, so-called multi-stage tests are performed. Here the increase of the vertical load is stopped when a certain strain level is reached. The pressure in the chamber is then increased and a new loading step is started using the same soil sample. Usually it remains unclear what the effect of the preceding step will be on the later test results.

In this programme, consolidated undrained (CU), single stage, triaxial tests were performed on 2 sets of clay samples. In Table 3.4 the sample numbers, the depths beneath the ground surface and the consolidation pressures (σ'_{co}) are given.

Table 3.4 Sample data triaxial tests

sample number	depth in m - ground level	σ'_{co} in kPa
3a	1.67 - 1.87	12
3b	1.87 - 2.07	18
3c	2.17 - 2.37	24
6a	5.10 - 5.30	20
6b	5.30 - 5.50	27
6c	5.50 - 5.70	33

The results of the tests on the samples 3a, b and c are presented in Fig. 3.4.
More extensive descriptions of the laboratory tests can be found in most major soil mechanical text books (e.g. Lambe and Whitman 1969), or in the soil laboratory test books of Head (1984, 1986, 1988).

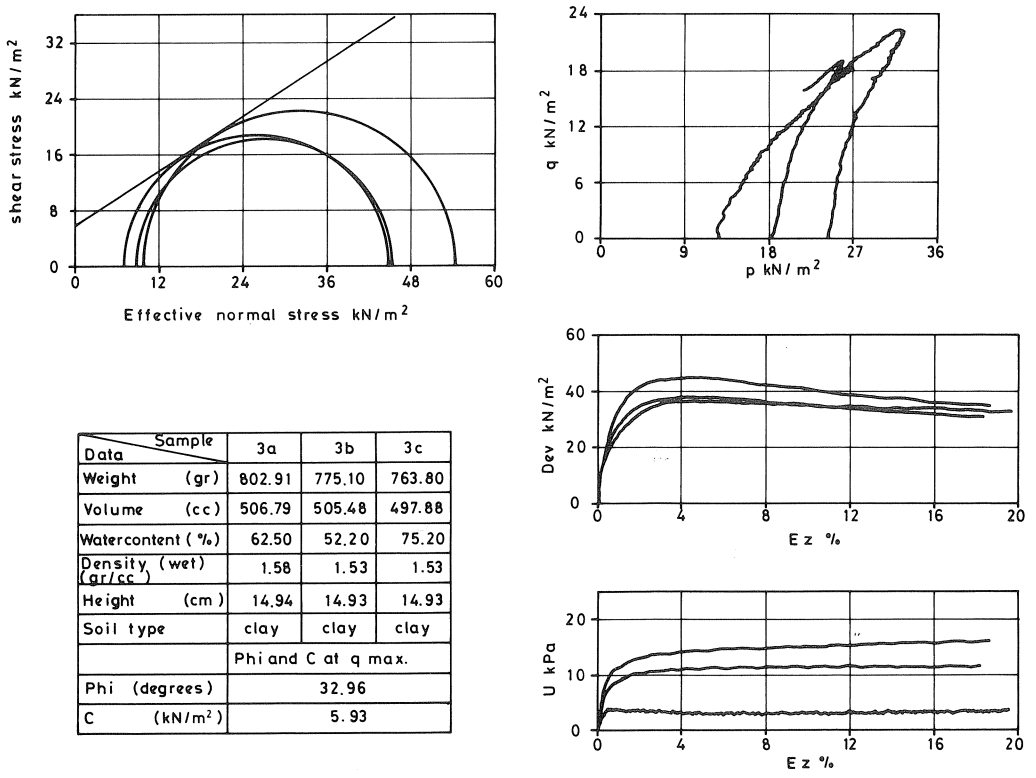

Data \ Sample	3a	3b	3c
Weight (gr)	802.91	775.10	763.80
Volume (cc)	506.79	505.48	497.88
Watercontent (%)	62.50	52.20	75.20
Density (wet) (gr/cc)	1.58	1.53	1.53
Height (cm)	14.94	14.93	14.93
Soil type	clay	clay	clay
	Phi and C at q max.		
Phi (degrees)	32.96		
C (kN/m²)	5.93		

Fig. 3.4 Triaxial test results samples 3a, b and c.

3.4 *Level 3: Pressuremeter tests*

The pressuremeter test is performed to establish the relationship between pressure and deformation of the soil, in situ. The test is performed by expansion of a cylindrical cavity formed in the ground. There are three major pressuremeter types. In the first type the pressuremeter is thrust to the required depth. In this case the soil is pushed aside just like during a cone penetration test. The second type is based on drilling a hole and lowering the pressuremeter into it. The third type is the self-boring pressuremeter. In this case a drill bit is incorporated within the pressuremeter.
After reaching the required depth the pressuremeter probe is inflated. This probe consists of a rubber membrane designed in such a way that an increase in volume is only possible by radial expansion. During the test both the pressure and the volume change are recorded.
The test is performed stress controlled; equal increments of stress are applied, and the stress levels are kept constant during one minute. Because the number of steps is usually between 8 and 14 the tests last 10 to 15 minutes. The test will therefore be undrained for clay and drained for sand.
From the test results, the Menard shear modulus, G, can be derived by constructing the tangent to the curve of the cell pressure as a function of $\Delta V/V_{present}$, where $V_{present}$ is the volume of the cell at the start of the pressure stap and ΔV the volume change during this step.
To obtain information about the undrained shear strength, the limit pressure, p_{lim}, is needed. This pressure can be extrapolated from the measured pressures. Usually this is done using a curve in which $\ln \Delta V/V_{present}$ is presented as a function of the cell pressure. Using cylindrical cavity expansion theory after Vesic (1972), c_u can than be derived from:

$$p_{lim} = \sigma_h + c_u \, (1 - \ln \, (G / c_u)) \tag{3.1}$$

where σ_h = the initial horizontal stress
During the first stage of this investigation level 8 mini-pressuremeter tests were performed at a distance of 2.0 m from the pile. The mini-pressuremeter, ø 24 mm, is driven into the ground by a hammer, so it is a soil-displacing pressuremeter.
In the second stage 8 additional tests were performed using a retrojet pressuremeter. This pressuremeter was lowered into a borehole, the diameter of the probe, 60 mm, is larger than that of the mini-pressuremeter. The maximum radial expansion is also larger. The tests were performed at the same depths as for the mini-pressuremeter.
The depths of both test series are presented in Table 3.5.
The depths of the tests were chosen based on the results obtained in the preceding stages of the soil investigations. All characteristic layers are tested except the layers beneath 8.0 m - ground level. This is due to the stiffness of these layers, which prevents penetration of the mini-pressuremeter.

The depths shown in Table 3.5 present the center of the pressuremeter.
Some characteristic results of the retrojet tests are shown in Fig. 3.5, 3.6 and 3.7.

Table 3.5 Depths of the pressuremeter tests

test number	depth in m - groundlevel
1	1.80
2	2.90
3	3.80
4	4.50
5	5.40
6	6.40
7	7.30
8	8.00

Presented are:
- Cell pressure as a function of $\Delta V/V_{present}$
- Shear modulus as a function of $\Delta V/V_{present}$
- ln $\Delta V/V_{present}$ as a function of cell pressure

Correction for membrane stiffness and thickness is already incorporated in the results presented here.
The results of the tests show that the values obtained by the mini-pressuremeter are higher than the values derived from the retrojet. This can possibly be explained by the different methods of installation of the pressuremeters. In case of the mini-pressuremeter the soil is deformed and compacted before starting the test, while for the retrojet a borehole is created and the soil adjacent to the borehole tends to expand and relax.

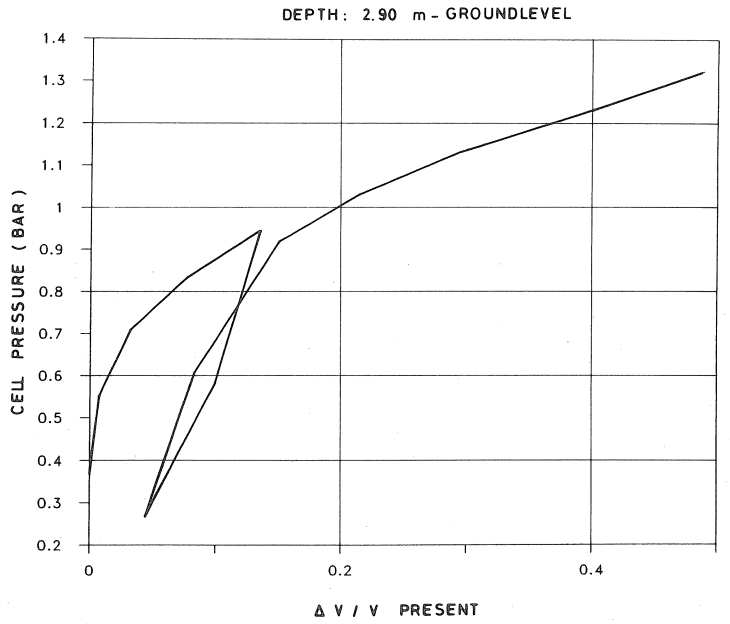

Fig. 3.5 Pressuremeter test result: pressure as a function of $\Delta V/V_{present}$.

An extensive description of the execution of the pressuremeter test, the design and construction of the probe, as well as the interpretation and use of the test results is given by Baguelin, Jézéquel and Shields (1978).
Full data of this part of the project are presented by Bijnagte and Berg, van den, (1988).

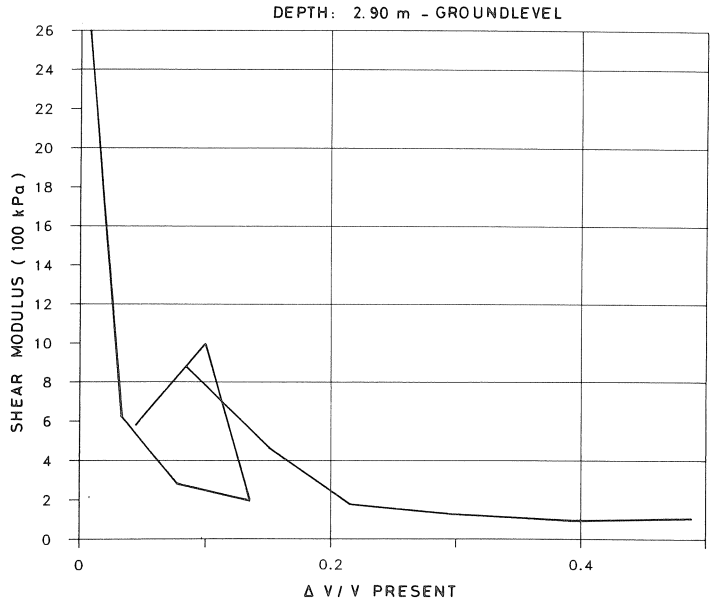

Fig. 3.6 Pressuremeter test results Shear modulus as a function of $\Delta V/V_{present}$.

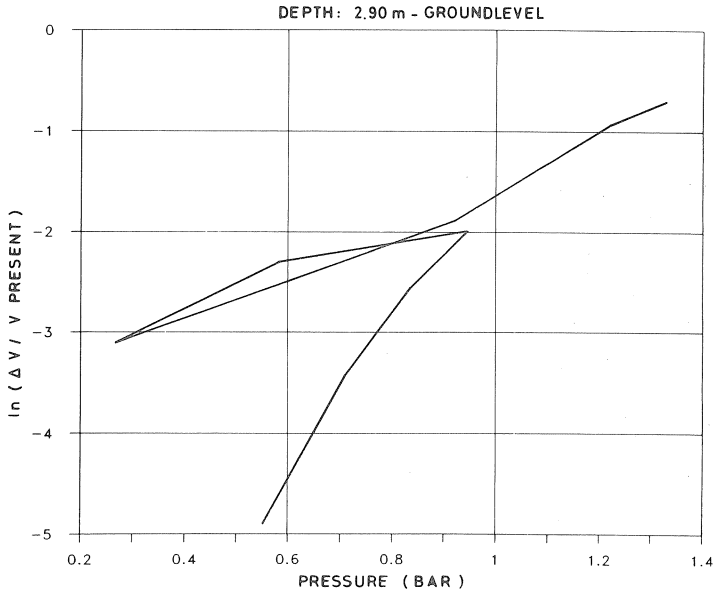

Fig. 3.7 Pressuremeter test result: ln $\Delta V/V_{present}$ as a function of pressure.

4 Discrete element model

4.1 *Introduction*

In this chapter the prediction of the laterally loaded pile and pile-soil behaviour using a discrete element model is presented. The pile, soil and its interaction are represented by discrete elements, such as lumped masses, springs and frictional elements.
A discrete element programme named TILLY was used, with which non-linear dynamic behaviour of structures can be modelled and simulated. This programme is being developed by the Mechanics & Structures Division of the Department of Civil Engineering of Delft University of Technology (Blaauwendraad and Kok, 1987).
The pile model consists of rigid elements connected with elastoplastic springs modelling the translational and bending behaviour of the pile at lateral loading. To model the pile-soil interaction, a new discrete element has been developed. This so-called HYGADE element describes the elastoplastic behaviour of the pile-soil interaction, the behaviour of the pile-soil interface and the degradation of the strength of the soil at cyclic pile loading. An important aspect of this interface behaviour is the so-called "gap" formation. A "gap" is a separation of the pile and the soil. At unloading of the soil backsliding of the gap may occur. This aspect is also modelled by the HYGADE element. An extensive description of this element is given by Grashuis (1988).
The constitutive model in the code allows the use of the models derived by Matlock (1970) and Sullivan et al. (1980). These models use a "*p-y* curve" approach and are accepted by the American Petroleum Institute, (API 1984), as well as Det Norske Veritas, (DNV 1977). The degradation of strength, the rate of the degradation process as well as the ultimate strength after infinite loading cycles can be included.

4.2 *Pile elements*

The pile was modelled by rigid body elements, interconnected by elastoplastic rotational springs, in Fig. 4.1 (a) represented by two parallel springs and a hinge. The degrees-of-freedom are located in the hinges. Using a sufficient number of elements and linear elastic springs it represents an Euler-Bernoulli-beam-model, neglecting shear deforma-

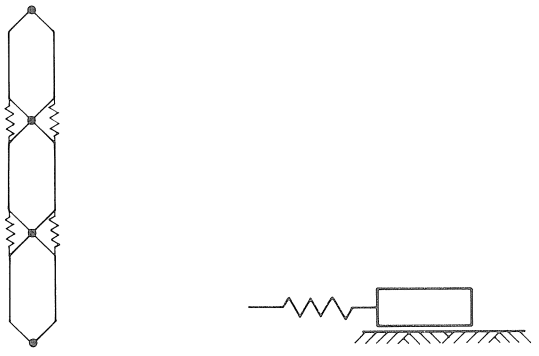

Fig. 4.1 Discrete element pile model (a) and dry friction element (b).

tion and effects of rotary inertia. Since the external loads for this application can be considered quasi-static, the model describes the pile behaviour sufficiently accurate in the frequency band of interest.
This model, as well as an extension inclusing shear deformation and rotary inertia (Timoshenko model), has been verified by extensive comparison of calculated results to static and dynamic tests, see Heinsbroek and Blaauwendraad (1989).
The parameters of the elements of the beam model have been derived from the distribution of mass and bending stiffness along the pile.

4.3 *Pile-soil interaction elements*

4.3.1 Static loading

The elastoplastic soil behaviour and the gap formation along the pile at some depth have been modelled by a spring and a massless dry friction element in series, see Fig. 4.1 (b).
This element reacts as a linear spring until the force reaches the threshold force of the friction element. Once this occurs the force in the spring will remain constant. In fact a one sided elastoplastic spring is modelled in this way. Both the stiffness of the spring and the slip force of the dry-friction element, which vary with soil type and depth, can be determined from the *p-y* curve approach.
The connection of the elements to the structural elements of the beam depends on the stress state in the springs. They can transfer compressional forces, and tensile stress up to a certain level. Exceeding the tensile threshold will result in a broken contact. During horizontal loading of the top of the pile, the elements representing the upper soil layers on the tensile side will lose contact. As soon as the threshold is exceeded a gap is originated on that side. Initial prestressing of the springs of the serial element, representing the horizontal stresses in the soil due to the soil weight, may be incorporated. This will affect the initiation of gap formation.
To model the non-linear *p-y* curves that describe the pile-soil interaction at a specific depth, a description by two of the serial elements parallel at each hinge was chosen, see Fig. 4.2. By choosing different yielding points and strengths of the elements, a tri-linear constitutive behaviour results, representing the *p-y* curves. An extensive description of this element is given by Grashuis (1988).

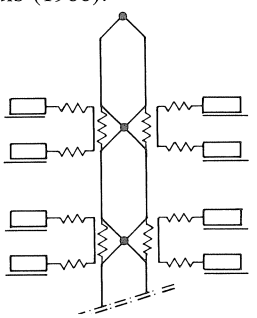

Fig. 4.2 Pile-soil interaction element.

4.3.2 Cyclic loading

For the case of cyclic loading of the pile additional properties have been added to the discrete pile-soil interaction model. As shown by the experiments of Matlock (1970), degradation of strength and stiffness and backsliding of the gap occurs. Further the pile wall will experience frictional forces due to the slip of the pile along the slot walls, see Fig. 4.3.

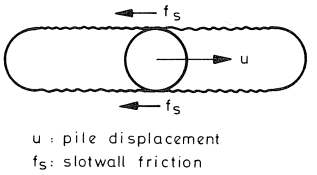

Fig. 4.3 Pile-slot wall friction.

The degradation of the soil strength has been modelled by two parameters: α and β. The parameter β models the decrease of the initial ultimate strength N_0 of the soil due to the loading cycles.
The ultimate strength of the soil after infinite loading cycles, N_{ul}, is defined as:

$$N_{ul} = (1-\beta)N_0 \qquad 0<\beta<1 \tag{4.1}$$

so βN_0 represents the decrease of the soil strength.
In general the parameter β is a function of the soil type, the plastic deformation, and the rate of loading.
By the parameter α the rate of degration is modelled. Using an exponential function this results in

$$N_{ul} = N_0 \{1-\beta\ (1-\exp(-\alpha n))\ \} \tag{4.2}$$

in which n is the number of cycles. Notice that for $\alpha = 0$ no degradation occurs. For $n = \infty$ and $\alpha = 0$ the ultimate strength, equation 4.1, results, see Fig. 4.4.
During cyclic loading the soil is first pushed forward into the displacement direction of the pile. After the pile has reached its maximum deflection and starts to move back tensile stresses between the pile wall and the soil will originate. Due to these stresses

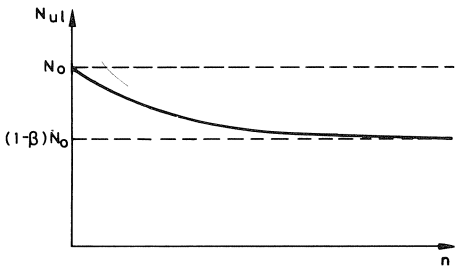

Fig. 4.4 Degradation function.

the soil will be pulled back, reducing the size of the gap. This phenomenon, called backsliding of the gap, is modelled with

$$Gap_i = \xi Gap_{i-1} N_{deg} / N_0 \tag{4.3}$$

in which N_{deg} is the strength of the degraded soil in the i-th cycle and Gap_i is the size of the gap in the i-th cycle. So backsliding of the gap for $\xi = 1$ is modelled to take place in proportion to the ratio of the present strength to the initial strength. By the parameter ξ the backsliding of the gap can be manipulated additionally.

4.4 *p-y curve approach*

4.4.1 Static loading

In this approach the soil along the pile is subdivided in different layers over the depth. For each depth a constitutive, design, relation between the soil resistance p per unit pile length and the horizontal displacement y of the pile at depth z has been derived by Matlock (1970), and Sullivan et al. (1980). Using these relations the stiffness and strength parameters of the discrete model can be derived. For clay the relation is determined by the following parameters of the soil in the layer: the undrained shear strength c_u at depth z, the density of the soil at that depth and the ε_{50} strain. This ε_{50} strain is defined as the strain corresponding to a stress level being half the maximum stress. Further the depth z and the pile diameter D are involved. These so-called p-y curves have been derived for different soil types, as soft and stiff clay as well as sandy soils, using experimental results as well as soil mechanical considerations. Fig. 4.5 shows a p-y curve for soft clay.

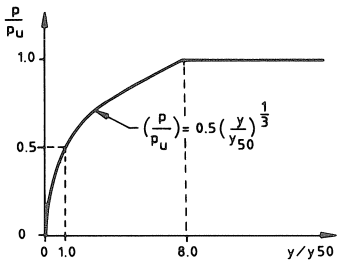

Fig. 4.5 p-y curve for soft clay.

4.4.2 Determination of the discrete pile-soil model parameters for static loading

The constitutive behaviour of the compressive force-displacement curve of the discrete model for the pile-soil interaction at some level z can be determined from the p-y curves by multiplying the soil resistance by the pile length involved. For the calculations the p-y curve of each layer has been approximated by two of the serial elements parallel to

each other. The maximum soil resistance of the two contributing elements 1 and 2 are respectively

$$N_{u1,1} = \frac{3}{7} p_{u1}\, dx \quad \text{and} \quad N_{u1,2} = \frac{4}{7} p_{u1}\, dx, \tag{4.4}$$

in which P_{u1} is the maximum soil resistance per unit pile length and dx is the length of the element.
The stiffnesses of the spring elements 1 and 2 are:

$$k_1 = \frac{3}{7} \frac{P_{u1}}{y_{50}} dx \quad \text{and} \quad k_2 = \frac{4}{7} \frac{P_{u1}}{8y_{50}} dx, \tag{4.5}$$

in which y_{50} is the displacement at half the maximum pressure.
In this way the path of the p-y curves is represented by the constitutive behaviour of the discrete model of the pile-soil interaction, see Fig. 4.6.

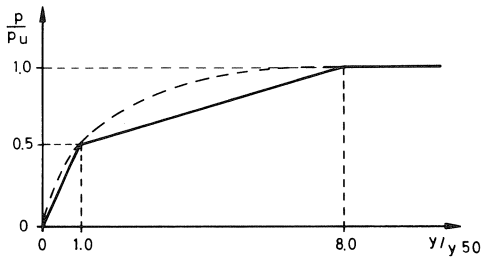

Fig. 4.6 Approximation of the p-y curve by two parallel springs.

This model for the pile-soil interaction has been verified extensively by comparison of calculated global lateral pile behaviour to measurements of static lateral pile-soil behaviour (Grashuis, 1988). The results were good.

4.4.3 Cyclic loading

The effects of cyclic loading of the pile on the pile-soil interaction as measured by Matlock (1970) have been implemented in the discrete model by the parameters α, β and ξ as discussed earlier.
Next to these effects the pile-slot-wall friction has been modelled by adding plastic springs, with a strength of 5% of the ultimate soil resistance, to the hinges at each level. The result of a calculation of the pile top displacement for a cyclic loading, is shown in Fig. 4.7, as well as the measurements of Matlock (1970). A comparison of the shape of the force-displacement relations shows that the model does represent the essential phenomena.

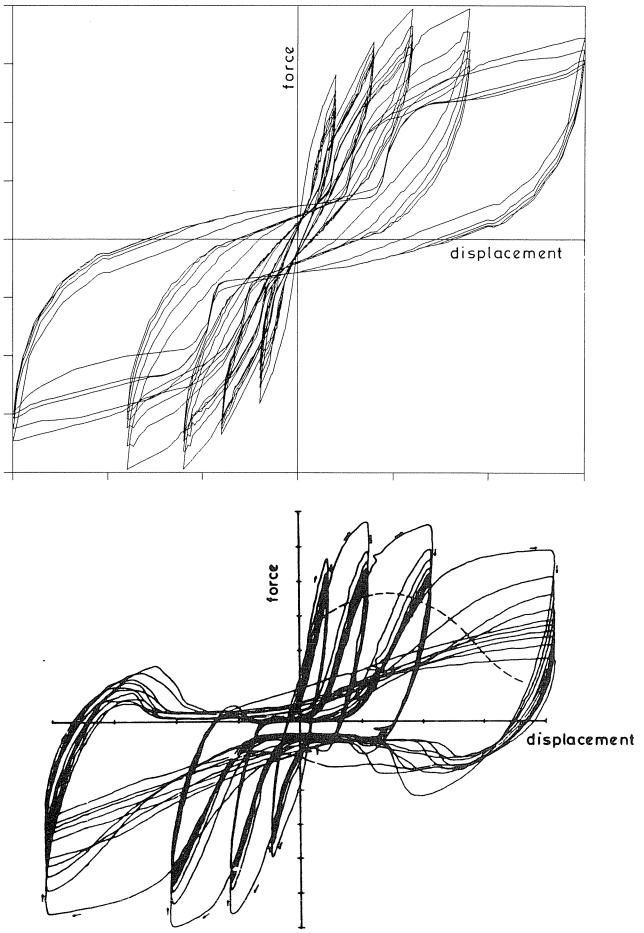

Fig. 4.7 Force displacement relation cyclically loaded soil, calculations (a) and experimental results (b).

4.5 *Predictions*

4.5.1 Discrete element model

The static behaviour of the test pile due to a lateral loading at the pile top has been determined using a discrete element model containing 17 degrees-of-freedom. The model is shown in Fig. 4.8.

4.5.2 Level 1 (CPT's)

An empirical relation between q_c and c_u widely used in engineering practice can be described in the following general form:

$$q_c = N_c \, c_u \tag{4.6}$$

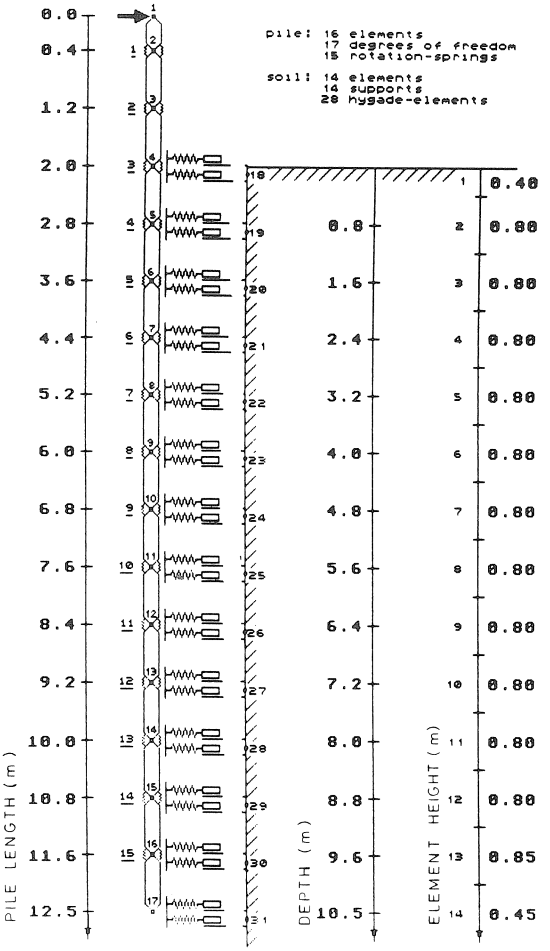

Fig. 4.8 Discrete element model of pile and soil.

where N_c is referred to as the cone factor. Most reported values for the cone factor are in the range between 10 and 20, see De Ruiter (1982). Recently, results of an Eulerean finite element model in which steady penetration is simulated showed that the factor is influenced by the roughness of the cone, the stiffness and strength parameters of the soft soil and the initial stress state (Berg, van den, 1991).
The range resulting from this numerical model corresponds well with the range from literature.

In this case, for both clay and sand layers, an "undrained shear strength" has been derived using a value of 15 for N_c in equation (4.6): $c_u = q_c / 15$. Speaking from a soil mechanical point of view, sand does not have an undrained shear strength, it behaves as a frictional material. In this case however, no distinction was made between clay and sand because the influence of the deeper sand layers was regarded to be relatively small.

The value for the ε_{50} strain has been chosen as 0.01, as suggested by Matlock (1970), for all layers. The horizontal effective stress in the soil increases with depth at an assumed rate of 4 kPa/m. The mean effective unit weight of the soil was assumed to be 7.5 kN/m^3. The diameter of the pile was taken as 0.66 m and its wall thickness as 9.2 mm, to account for the additional effect of the U profiles on the pile wall. The bending stiffness amounts to 210 MNm^2. The values mentioned determine the parameters of the pile and pile-soil model. The calculated load-pile top displacement is presented as graph 1 in Fig. 4.9.

4.5.3 Level 2 (boring and laboratory tests)

For the layers between ground level and 6.8 m - ground level the undrained shear strength has been determined from the vane tests. Comparison of the c_u values from the vane tests with those following from the cone penetration tests indicates that the N_c value of 15 is too small for the peat layers. Values in the order of 20 should be used. Triaxial tests have been used to determine the ε_{50} strain. The main value derived is: $\varepsilon_{50} = 0.005$ for each depth, whereas in the calculations of level 1 a value of 0.01 was chosen. Thus the stiffnesses derived for the springs of the serial elements are doubled with respect to level 1, the ultimate strength is almost the same (Grashuis, 1989). The

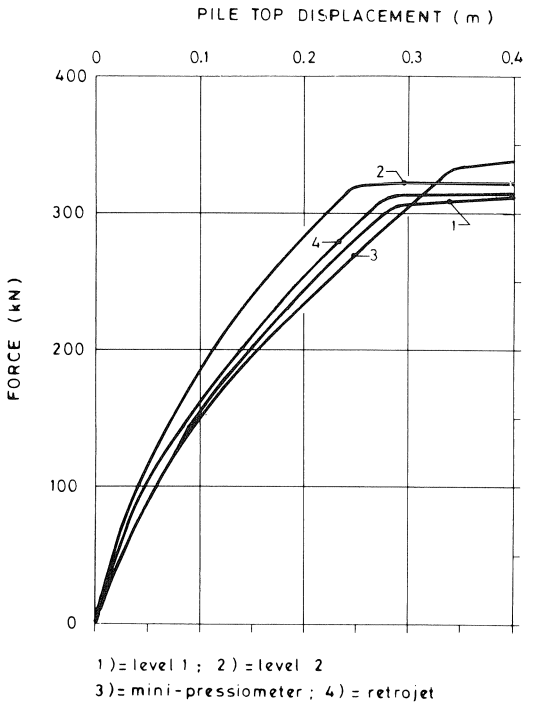

Fig. 4.9 Force-displacement relations discrete element calculations.

resulting load-pile top displacement is given as graph 2 in Fig. 4.9. The pile-soil behaviour is 20% stiffer than in level 1. The pile model is calculated to fail at a load of 324 kN. In level 1 no yielding of the pile was taken into account.

4.5.4 Level 3 (pressuremeter tests)

From the presented graphs, the Young's modulus, E, and the undrained shear strength c_u at each depth have been derived. Assuming continuous elastic behaviour the Young's modulus follows from the shear modulus as:

$$E = 2\ (1 + \nu)\ G \tag{4.7}$$

For an undrained Poisson's ratio ν of 0.5, this results in $E = 3G$. From the pressuremeter tests, the Young's modulus and the c_u are known at eight depths. By averaging the values over the layers, the stiffnesses and strengths of the elements have been determined for the upper 9 serial elements of the calculation model. The Young's modulus was used to determine the stiffness of the p-y curve at $y = 0$. From this the ε_{50} value was derived with

$$\varepsilon_{50} = (0.5\ p_{u1} dx) / (2.5\ E\ D^2) \tag{4.8}$$

For the mini-pressuremeter tests this resulted in rather large values of the ε_{50} strains, $0.01 < \varepsilon_{50} < 0.014$. These values are explained by the relatively small values derived for the Young's moduli.
In case of the retrojet test the Young's moduli derived were substantially higher, however still small, and resulted in ε_{50} values between 0.003 and 0.024.
The resulting load-pile top displacement is presented in Fig. 4.9 in graph 3 for the mini-pressuremeter tests and for the retrojet tests in graph 4. The graphs show that the stiffness of the pile-soil interaction has been reduced considerably in the prediction based on the mini-pressuremeter data. The result for the retrojet data is located between the graphs derived in level 1 and 2.

4.5.5 Final prediction

Rather large differences for the undrained shear strength, c_u, and ε_{50} strain result from the soil investigations in the three levels. These differences are less visible in the pile-top displacement since the bending stiffness of the pile plays an important role in the overall behaviour and this parameter is constant in all calculations. The same applies to the soil layers at the lower part of the pile which are relative stiff and strong in all cases. Based on engineering judgement the soil data were arranged in order of decreasing reliability as:
- cone penetration test and retrojet tests;
- cone penetration test and boring with laboratory tests (vane tests);
- cone penetration test;
- cone penetration test and mini-pressuremeter tests.

In the final prediction the soil data derived from the retrojet tests have been used. The data used are presented in Table 4.1:

Table 4.1 Data used for the final prediction

element nr. [–]	element length [m]	mean shear strength [kN/m^2]	ε_{50} [–]
1	0.40	22.5	0.0028
2	0.40	24.5	0.0074
3	0.80	24.0	0.0083
4	0.80	20.0	0.0075
5	0.80	18.5	0.0075
6	0.80	25.0	0.011
7	0.80	32.0	0.012
8	0.80	42.5	0.015
9	0.80	49.0	0.024
10	0.80	109.3	0.010
11	0.80	76.7	0.010
12	0.80	70.0	0.010
13	0.85	220.0	0.010
14	0.45	256.7	0.010

For this case the following graphs are given:
- Force-pile top displacement, Fig. 4.10;
- Displacement of the pile at all levels, Fig. 4.11;
- Bending moment distribution, Fig. 4.12;
- Bending moment-force diagram, Fig. 4.13.

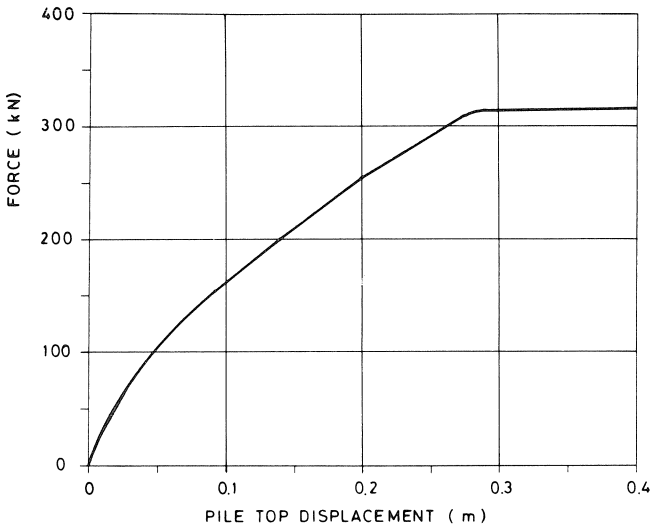

Fig. 4.10 Force-pile top displacement, final prediction.

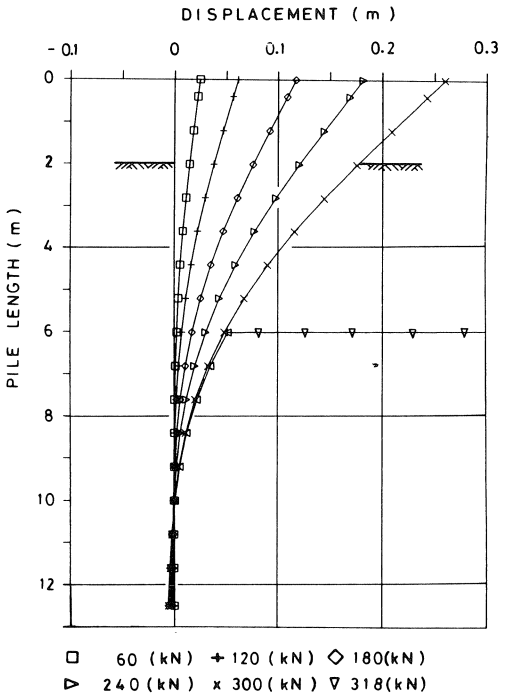

Fig. 4.11 Displacement of the pile at all levels, final prediction.

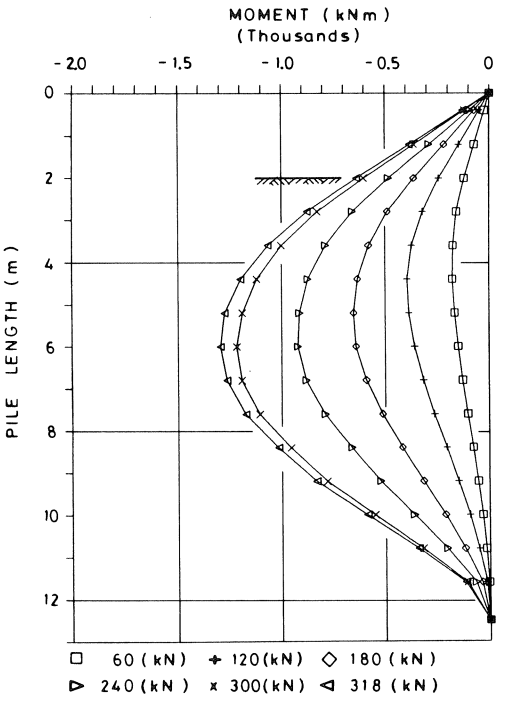

Fig. 4.12 Bending moment distribution, final prediction.

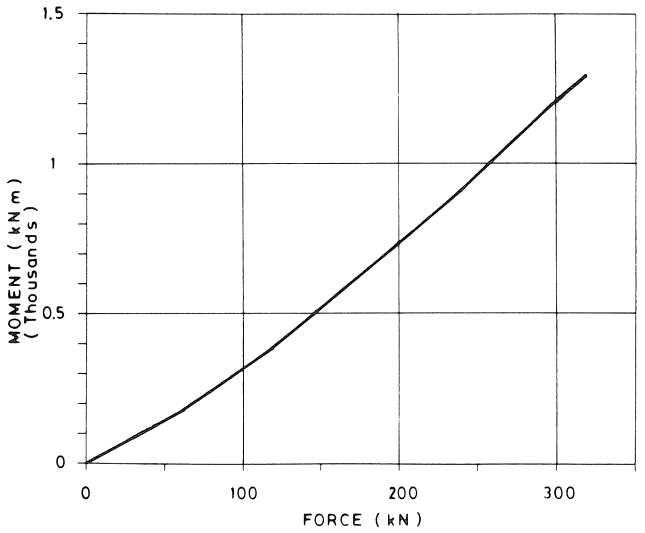

Fig. 4.13 Bending moment-force diagram, final prediction.

4.5.6 Cyclic prediction

The cyclic behaviour of the pile and pile-soil interaction was estimated using the soil data as derived from the retrojet tests.
To predict the cyclic behaviour, some cyclic calculations were performed. They show the degradation of strength and stiffness that might be measured. Five different cyclic calculations of six cycles each have been performed with different values of α and β. The values used are presented in Table 4.2. In all cases for ξ a value of 0.2 was used.

Table 4.2 Parameters used in cyclic calculations

Case	α	β
1	0.5	0.6
2	0.25	0.6
3	1.0	0.6
4	0.5	0.4
5	0.5	0.8

The maximum cyclic load in these calculations was 125 kN. The following graphs are depicted:
- displacement distribution along the pile at maximum loading in each cycle for case 1 is shown in Fig. 4.14;
- force-pile top displacement in each cycle for case 1, Fig. 4.15.

Results of the other cases are presented by Grashuis (1989). The calculations performed were not intended to make realistic predictions for the test series, since there is little experience with this kind of calculation. A comparison between the calculations and

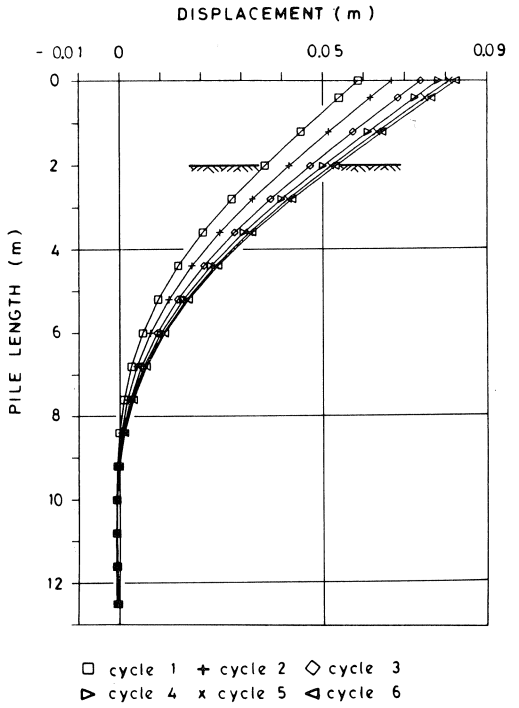

Fig. 4.14 Displacement distribution along the pile at maximum loading in each cycle for case 1 of Table 4.2.

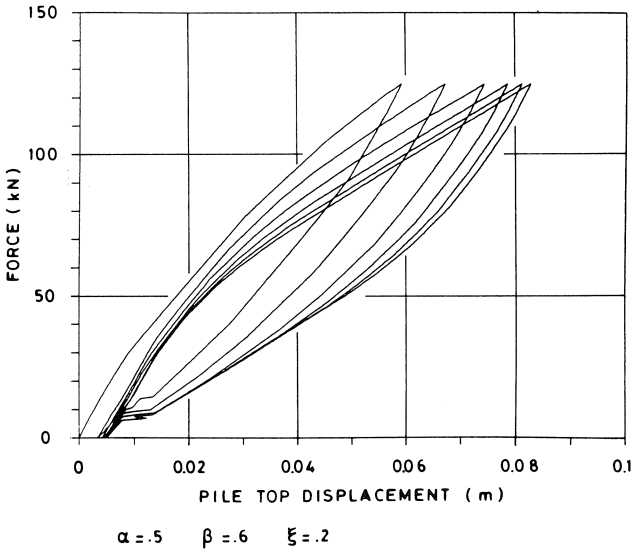

Fig. 4.15 Force-pile top displacement in each cycle for case 1 of Table 4.2.

the test results shows which parameter values give a satisfying agreement for this specific situation, when the parameter values are considered to be the same for all soil layers. For other conditions different values may apply.

5 Quasi 3-dimensional model

5.1 *Introduction*

In this part the application of the quasi 3-dimensional numerical model, the computer programme LPG: Laterally Loaded Pilegroup, will be presented. The rationale for the development of this model is the use of a continuum approach, in which the distribution of the stresses and deformations in the soil can be represented in a more correct way than in the discrete element modelling used in the foregoing chapter. The advantage of the continuum model is the direct use of physical quantities for the soil properties, such as Young's modulus and Poisson's ratio. Also, there is the possibility of modelling the local pile-soil interaction. Disadvantages of such a model are the memory requirements for the computer and the long run times of the programme. These disadvantages have been reduced by partitioning the 3-dimensional analysis into a series of 2-dimensional analyses.
In the case of a laterally loaded pile, the lateral displacements in the soil will prevail over the vertical displacements. Further assuming that the vertical stresses in the soil are hardly affected by the horizontal displacements in the soil, the soil can be modelled by a system of continuous disks, see Fig. 5.1. These disks are coupled in the vertical direction by an iterative process in which the behaviour of the layers is calculated using a finite element method. The only stress components that can be transferred from one disk to another are shear stresses in a horizontal plane. For a linear stress-strain relation in the continuum this process has been described by Verruijt and Kooijman (1989). Plasticity is confined to horizontal layers (Kooijman and Vermeer, 1990). To model plasticity, the Tresca yield criterion is used (Tresca, 1868). This implies that for material with frictional behaviour a transformation of the stress parameters to a Tresca model has to be made. In this case, for the sand layers, the failure load of sand with an angle of

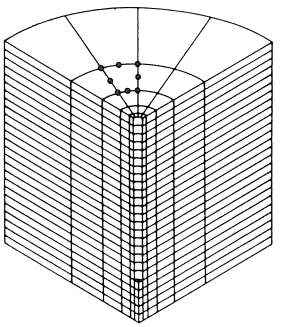

Fig. 5.1 Layer system of the quasi 3-dimensional model.

internal friction of 35° was calculated according to the API code (1984). Using the API method for clay the undrained shear strength resulting in an equal failure load was derived and used for further calculations.
The local contact between pile and soil is modelled by an interface element allowing slip between pile wall and soil. The element allows to introduce a limited tensile stress so that gap formation can be modelled. The interface element has been described by Kooijman (1989a). The model has been verified by other 3-dimensional calculations as well as simulations of tests.
A complete description of the model, has been given by Kooijman (1988).

5.2 *Predictions*

5.2.1 Level 1 (CPT's)

The undrained shear strength c_u was derived from the cone resistance q_c by equation (4.6). In this case c_u was also taken as $q_c/15$.

The shear modulus G was estimated as

$$G = 100\ c_u \tag{5.1}$$

Poisson's ratio ν was taken as ≈ 0.5. The horizontal effective stress in the soil has been estimated as 0 at the bottom of the pit with a linear increase of 4 kPa/m depth below the bottom of the pit.
The pile was considered to be rough with respect to slip between the pile wall and the soil, this means that no slip would occur. In order to allow gap formation the soil along the pile wall could not transfer tensile stresses.

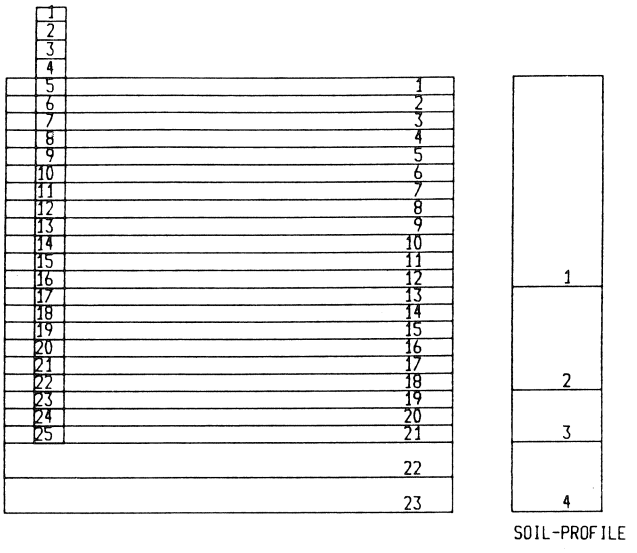

Fig. 5.2 Soil profile prediction level 1.

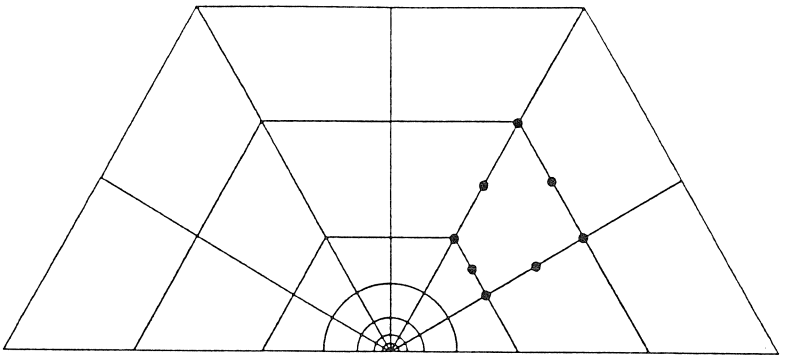

Fig. 5.3 Soil layer finite element mesh quasi 3-dimensional model.

The pile was divided into 25 elements of 0.5 m each and the soil from pit bottom to pile tip into 21 layers of 0.5 m. Two layers of 1 m each below the pile tip finish the soil discretization, as shown in Fig. 5.2. The soil above the pit bottom was disregarded, with respect to the effect of its weight. The mechanical soil properties were derived for the original groundlevel. The influence of the relatively small excavation around the pile top on the behaviour of the soil layers is assumed to be negligible. The parameter values used in this calculation level are presented in Table 5.1. The finite element mesh of a layer used in these calculations is shown in Fig. 5.3. The values of the pile model parameters used are: $D = 0.66$ m and a wall thickness $s = 9.2$ mm, these values are used to compensate for the steel profiles connected to the pile.

The resulting load-displacement curve for level 1 is presented as graph 1 in Fig. 5.4. The force at which the pile starts to fail is about 230 kN.

The maximum bending moment before yielding would occur is calculated as 720 kNm.

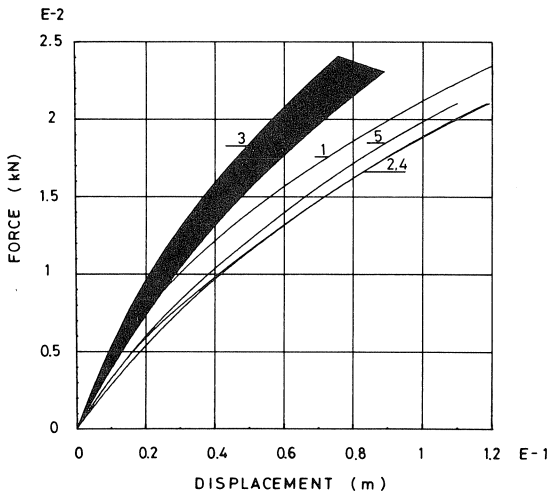

Fig. 5.4 Force-displacement relations quasi 3-dimensional model calculations.

Table 5.1 Data used in quasi 3-dimensional model calculations

		depth below the bottom of the pit in m	E modulus in kPa	cohesion in kPa	horizontal effective stress in kPa
Level 1	layer				
	1	0.0–6.0	6000–6000	20–20	0.0–30.0
	2	6.0–9.0	20000–20000	65–65	30.0–45.0
	3	9.0–10.5	60000–60000	200–200	45.0–52.5
	4	10.5–12.5	20000–20000	65–65	52.5–62.5
Level 2	layer				
	1	0.0–1.2	6000–6000	20–20	0.0–4.8
	2	1.2–3.2	1800–1800	30–30	4.8–12.8
	3	3.2–6.5	6000–9000	20–30	12.8–26.0
	4	6.5–9.5	24000–24000	80–80	26.0–38.0
	5	9.5–11.0	45000–45000	200–240	38.0–44.0
	6	11.0–12.5	20000–20000	65–65	44.0–50.0
Level 3a	layer				
mini pressure	1	0.0–1.2	10800–10800	36–36	0.0–4.8
meter	2	1.2–3.0	12900–12900	43–43	4.8–12.8
(G/cu = 100)	3	3.0–6.5	12000–19500	40–65	12.8–26.0
	4	6.5–9.5	24000–24000	80–80	26.0–38.0
	5	9.5–11.0	45000–45000	200–240	38.0–44.0
	6	11.0–12.5	20000–20000	65–65	44.0–50.0
Level 3b	layer				
mini pressure	1	0.0–1.2	5400–5400	36–36	0.0–4.8
meter	2	1.2–3.0	6450–6450	43–43	4.8–12.8
G/cu = 50)	3	3.0–6.5	6000–9750	40–65	12.8–26.0
	4	6.5–9.5	24000–24000	80–80	26.0–38.0
	5	9.5–11.0	45000–45000	200–240	38.0–44.0
	6	11.0–12.5	20000–20000	65–65	44.0–50.0
Level 3c	layer				
retrojet	1	0.0–1.2	3000–3000	20–20	0.0–4.8
	2	1.2–3.0	2400–4650	30–30	4.8–12.8
	3	3.0–6.5	3000–7500	20–50	12.8–26.0
	4	6.5–9.5	24000–24000	80–80	26.0–38.0
	5	9.5–11.0	45000–45000	200–240	38.0–44.0
	6	11.0–12.5	20000–20000	65–65	44.0–50.0
Final	layer				
prediction	1	0.0–1.2	4500–4500	20–20	0.0–4.8
	2	1.2–3.0	2400–4650	30–30	4.8–12.8
	3	3.0–6.5	4500–11250	20–50	12.8–26.0
	4	6.5–9.5	24000–24000	80–80	26.0–38.0
	5	9.5–11.0	45000–45000	200–240	38.0–44.0
	6	11.0–12.5	20000–20000	65–65	44.0–50.0

a–b: "a" at the top of the layer and "b" at the bottom of the layer.

5.2.2 Level 2 (boring and laboratory tests)

The soil profile derived from the boring is depicted in Fig. 5.5. It was refined in order to take the layering of the soil, according to the Delft Continuous Sampler, into account. Additionally, in this investigation level an empirical relation based upon the plasticity index for soil strength and stiffness parameters is used (Terzaghi and Peck, 1967):

$$c_u = (0.11 + 0.37\ \mathrm{PI})\sigma'_v \tag{5.2}$$

$$G = (10 - 15\sigma'_i)/(\mathrm{PI}), \tag{5.3}$$

with

σ'_i = effective isotropic stress
σ'_v = effective vertical stress
PI = plasticity index

Using these equations for the different clay layers the G/c_u ratio of 100 that was chosen in the first calculation proved to be correct and was used again. However for the peat layer at 1.2 m–3.2 m below the bottom of the pit, the simple shear test resulted in a value of about 20. For the calculations this ratio was used. However for the c_u values, the values derived from the cone penetration tests for the clay and peat layers were used again. The strength of the sand layer at 9.5 m to 11 m below the pit bottom was derived in a different way. The yielding pressure calculated according to the rules of the API is determined with an estimated angle of internal friction of 35°, a K_0 of 0.6 and an effective unit weight equal to 5 kN/m^3 for the first 9.8 m and 7.5 kN/m^3 for the deeper layers. A constant value for Young's modulus of sand equal to 45 MPa was chosen. The parameter values used are given in Table 5.1. The other parameters are the same as in

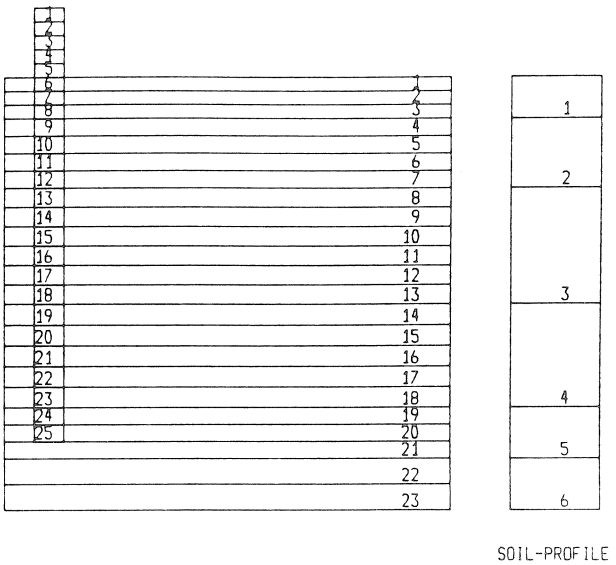

Fig. 5.5 Soil profile prediction level 2.

level 1. The load-displacement curve in Fig. 5.4, graph 2, shows that the stiffness is smaller than in the first calculation. The calculated load at which yielding of the pile occurs is now 210 kN.

5.2.3 Level 3 (pressuremeter tests)

The interpretation of the mini-pressuremeter tests resulted in very small values for the shear modulus and slightly higher values for the undrained shear strength when compared with previous values. The ratio of G/c_u, which is between 50 and 200 in normal situations, was found to be considerably smaller than 50 now. Since the c_u values derived from the mini-pressuremeter test were assumed to be realistic for the soil layers up to 6.5 m below the pit bottom, they have been used. The values for the shear modulus G have been raised, such that $G/c_u = 50$ to 100, and both extremes have been used in a calculation. The relevant soil properties are presented in Table 5.1 as "Level 3a" and "Level 3b". The soil profile is the same as in level 2. The load-displacement curves following from these data define the boundaries of the black area "3" in Fig. 5.4. The higher values of the shear moduli result in stiffer pile-soil behaviour than in the other calculations. At maximum load the pile top displacement found was 75–90 mm, which is considerably smaller than the 120 mm found in the other calculations.
Young's moduli derived from the retrojet test were substantially higher and more realistic. Therefore these values were not raised, although they were still small compared to the ones derived from the cone penetration tests. The data have been given in Table 5.1 under "Level 3c". The calculated load displacement curve is shown as graph 4 in Fig. 5.4. The results of this calculation are almost equal to those of the level 2 calculation.

5.2.4 Final prediction

A final prediction was calculated using all the available soil data. This calculation started with data based on the retrojet calculation. However, an increased shear modulus of 75 times c_u, which is in accordance with the plasticity index measured in level 2, was used.
All other soil data were left unchanged, see Table 5.1. The final load displacement function is depicted as graph 5 in Fig. 5.4.
Plots of the displacement, bending moment and soil pressure distribution at a load of $F = 105$ kN and at the maximum load $F = 210$ kN are given in Fig. 5.6, 5.7 and 5.8. p-y curves at four levels have been derived based on the calculated soil reactions, see Fig. 5.9. For more detailed information see Kooijman (1988).

5.2.5 Cyclic prediction

In the graph of Fig. 5.10 the calculated unloading-reloading curve is presented by the dashed line. The predicted hysteresis is small. This can be explained by the fact that a

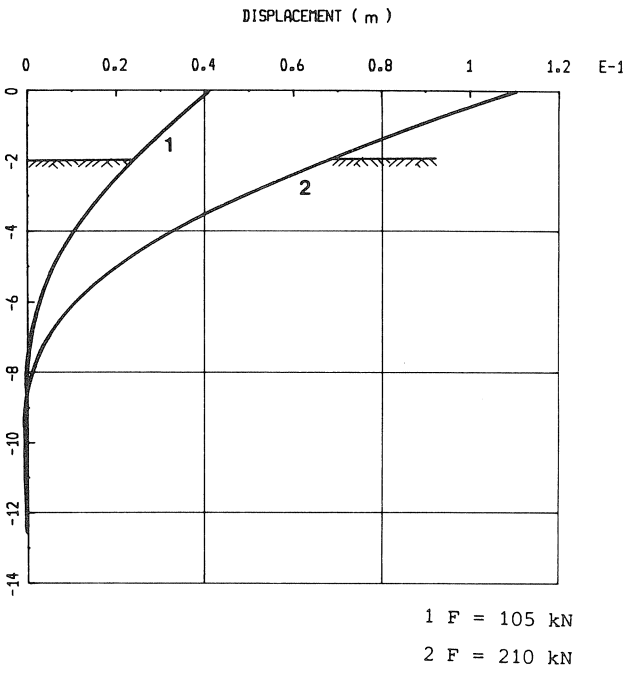

Fig. 5.6 Pile displacement quasi 3-dimensional model, $F=105$ kN and $F=210$ kN, final prediction.

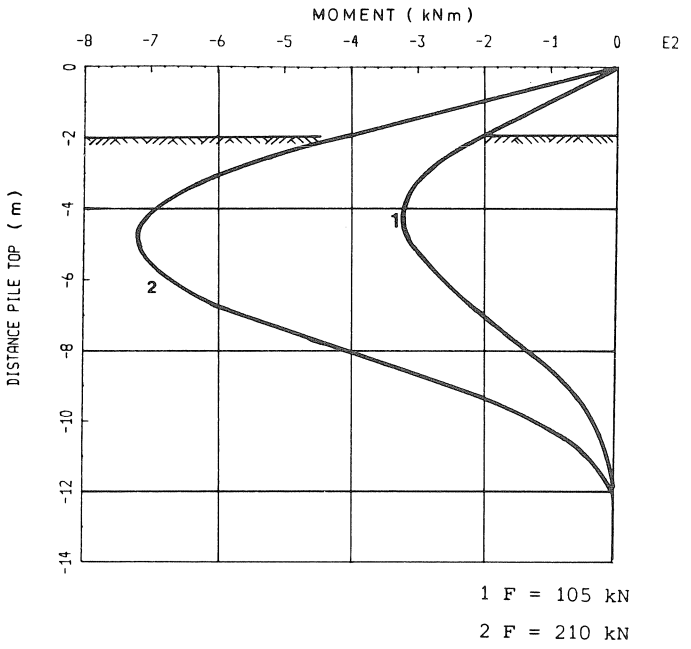

Fig. 5.7 Bending moment distribution quasi 3-dimensional model, $F=105$ kN and $F=210$ kN, final prediction.

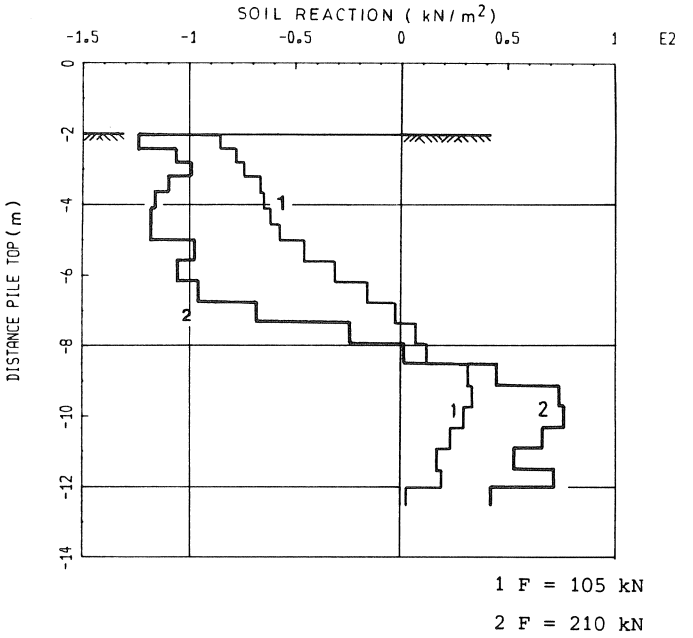

Fig. 5.8 Soil pressure distribution quasi 3-dimensional model, $F=105$ kN and $F=210$ kN, final prediction.

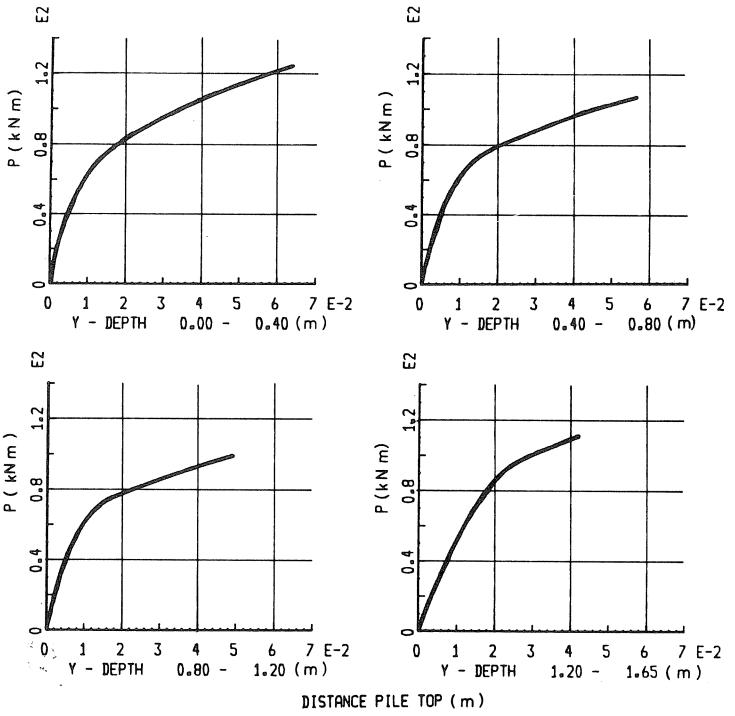

Fig. 5.9 Calculated *p-y* curves quasi 3-dimensional model, final prediction.

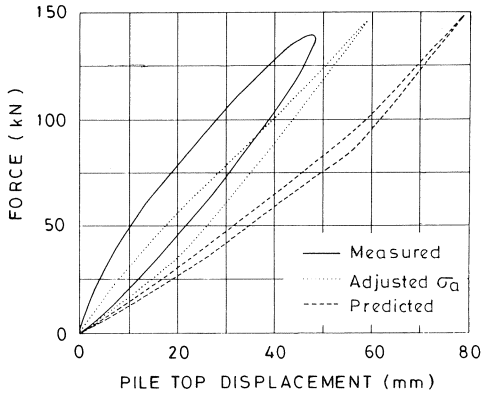

Fig. 5.10 Pile top displacements for cyclic loads.

gap is supposed to originate at zero tensile strength of the pile-soil contact surface, therefore very little energy is needed to create the gap. After the field test was carried out another cyclic calculation, in which adhesion between the pile and the soil was included, was performed. The adhesion was assumed to be equal to the undrained shear strength. This results in a much higher energy dissipation, as presented by the dotted line in Fig. 5.10. Apparently a variation of the value of the adhesion significantly influences the dissipated energy.

6 3-Dimensional Finite Element analyses

6.1 *Introduction*

As a result of the continuous development of hardware and software applications it is now possible to perform fully 3-dimensional non-linear finite element analyses for a horizontally loaded single pile without super-computer or unrealistic CPU time requirements. In contrast to a 2-dimensional or axi-symmetric approach, in fully 3-dimensional calculations no assumptions have to be made for specific components of the stress tensor, σ_{ij}; the complete set of 3-dimensional equilibrium equations is used. In the analyses presented in this chapter the general purpose finite element code DIANA of TNO Building and Construction Research (TNO-BOUW) was used.
Generally in geomechanics a 2-dimensional, plane strain or axi-symmetric, approach is applied. Therefore, it is useful to consider the following points prior to starting a 3-dimensional analysis:

a. *The large number of elements and integration-points.*
Based on a 2-dimensional rectangular mesh containing $n \times n$ elements, where n is the number of elements on one side of the mesh, the same cubic mesh contains n^3 elements. So, for n equal to ten, which resembles a very coarse mesh of 100 elements

in a 2-dimensional model the corresponding 3-dimensional case requires 1000 elements. Considering the number of integration points the increase is even larger. Full integration of second order elements in the 2-dimensional case requires 900 integration-points whereas in the 3-dimensional case the stresses of 27000 Gaussian points have to be calculated. Needless to mention that the number of nodal points, better: the number of degrees-of-freedom, the bandwidth of the system matrix, and the memory requirements of the computer also increase substantially.

b. *Model check, interpretation and presentation of the results.*
In contrast to a 2-dimensional analysis, the enormous quantity of data requires a professional pre- and post-processing programme in order to produce input and handle results. This includes graphical, on-screen, checks of the mesh and boundary conditions and presentation of the calculated stress and strain distributions as coloured isoline-plots. PATRAN was used in the analyses presented. PATRAN is a registered trademark of PDA Engineering.

c. *Test runs.*
More than in a 2-dimensional analysis it is recommended that test runs be performed, before starting the final analysis, in order to check the element and global model behaviour. In this case a very coarse model consisting of only ten solid and eight shell elements was used. All important features, for example plasticity and interaction between pile and soil, were incorporated and the complete scope of the analysis was carried out. The final calculation model was built upon the evaluation of the results of the test run.

The model utilized twenty-noded hexahedron elements and eight-noded cylindrical shell elements. Special attention was paid to the behaviour at the interface: the interaction mechanism. The constitutive behaviour of both soil and pile was described by a "perfect elastic-perfect plastic" material model, see Fig. 6.1, no hardening or softening is taken into account.

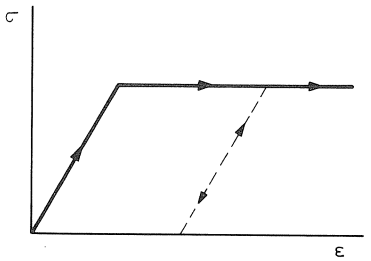

Fig. 6.1 Stress-strain behaviour of a perfect elastic-perfect plastic material.

6.2 *Elements*

6.2.1 Pile elements

Eight-noded quadratic Serendipity, degenerated, shell elements were used to model the pile. The cylindrical geometry of this element is used to model the thin-walled pile.

The element has five degrees of freedom per node; three translations and two rotations, sufficient for an at least linear strain distribution within the element. To avoid shear and membrane locking, a reduced integration scheme was applied: two-by-two Gaussian integration. However, it is known that locking effects cannot be completely excluded; a somewhat too stiff behaviour of this element type could therefore occur.

6.2.2 Soil elements

Twenty-noded quandrilateral hexahedrons were used to model the soil. This element is an iso-parametric Serendipity element with sixty degrees-of-freedom: translations in x, y and z direction at each node. The strain distributions are at least of lineair order within the element. A reduced Gaussian integration scheme with eight integration points was applied for the numerical integration of the element. This reduced integration usually renders results closer to reality than full integration since it results in a system with less constraints.

6.3 *Material behaviour*

6.3.1 Soil

The behaviour of the soil, both granular and cohesive, is modelled using "perfect elastic-perfect plastic" constitutive models. Thus, no hardening effects will be taken into account. The material is assumed to have lineair elastic behaviour up to the yield surface.

Two basically different soil reactions can be distinguished: drained and undrained behaviour, depending on loading rate and permeability. Drained behaviour implies that the pore-water in the deformed soil has the possibility to flow to other regions, whereas undrained behaviour assumes that this is not possible: the soil volume is constant.

In reaction to the relatively short-term loading considered in this project, soft cohesive soils layers, clay and peat, will behave undrained whereas the granular sandy soil layers, due to the relative high permeability, show a drained behaviour.

The undrained plastic behaviour of the clay and peat was modelled by the Tresca material model (Tresca, 1868). This implies that the difference between the maximum and minimum principle stresses in the soil has a maximum value equal to two times the undrained c_u of the soil (shear strength):

$$\max\left[|\sigma_1-\sigma_2|,\quad |\sigma_2-\sigma_3|,\quad |\sigma_3-\sigma_1|\right] \leqq 2c_u \tag{6.1}$$

The yield surface for the drained behaviour of the sandy layers is modelled by a combination of the Mohr-Coulomb model (1776) and the tension cut-off criterion according to Rankine (1857):

$$\sigma_1(1+\sin\phi)-\sigma_3(1-\sin\phi) \leqq 2\ c\cos\phi \tag{6.2}$$

and

$$\max\left[\sigma_1, \sigma_2, \sigma_3\right]=f_t \tag{6.3}$$

where:

c = cohesion of the soil
ϕ = angle of internal friction
f_t = maximum tensile stress, often taken equal to the cohesion

A non-associated flow rule is used. So for the soil layers an additional parameter has to be introduced: the dilatancy angle ψ (Vermeer and De Borst, 1984).
The programme version used for the calculations did not support facilities to introduce an initial stress state. The soil was therefore assumed to be initially stress free. This is a reasonable assumption for the soft soil layers, since the yield stress is not dependent on the isotropic stress. However, for the, deep, sand layers this may result in too soft behaviour.

6.3.2 Pile

The constitutive behaviour of the steel pile is assumed to be linear elastic up to the yield value. The perfectly plastic yield surface is modelled by the Von Mises criterion, characterized by the 1-dimensional yield stress σ_y:

$$(\sigma_1 - \sigma_2)^2 + (\sigma_2 - \sigma_3)^2 + (\sigma_3 - \sigma_1)^2 \leqq 2\sigma_y^2 \tag{6.4}$$

6.3.3 Interface pile-soil

Experience with 2-dimensional calculations has shown that it is very important to model the behaviour at the interface between a construction and soil in a correct way. When large localized strains are involved, special elements are needed to correctly describe the interface behaviour. Two mechanisms can be distinguished at the interface: the contact-gapping mechanism and the frictional shearing mechanism.
Three kinds of interface constitutive equations can be used for numerical simulations (Boulon and Nova, 1990). The simplest equation models the frictional contact between two solids by means of a rigid-perfectly plastic, Coulomb condition. Another approach is to consider the soil-structure interface as a thin continuum layer. The third approach replaces the interface zone with a bi-dimensional constitutive relation (Boulon, 1989). In this case the interface behaviour between pile and soil is described in terms of a relation between the normal and shear tractions, t_n and t_s, and the normal and shear relative displacements across the interface, Δu_n and Δu_s. In geomechanics, when the stresses are within the elastic region, the normal and shear relations are generally assumed to be independent:

$$\begin{vmatrix} t_n \\ t_s \end{vmatrix} = \begin{vmatrix} D_{11} & 0 \\ 0 & D_{22} \end{vmatrix} \begin{vmatrix} \Delta u_n \\ \Delta u_s \end{vmatrix} \tag{6.5}$$

In this matrix D_{11} stands for the relation between normal traction and normal relative displacement: the contact-gapping mechanism.
D_{11} resembles an elastic spring stiffness, a very stiff spring to simulate contact up to a

specified maximum tensile stress. If the tensile stress exceeds this threshold value a discrete "gap" arises between pile and soil and the tensile stress reduces to zero: instantaneous, linear or non-linear.

Generally the friction mechanism, D_{22}, is described as follows: up to a specified shear stress, depending on the normal stress at the interface, "elastic" shear-behaviour is assumed. If the shear stress exceeds this threshold plastic slip deformation occurs at the interface. In that case the maximum shear stress τ_{max} can be defined by the Coulomb friction model (1776):

$$\tau_{max} = a + \sigma_n \tan \delta$$

where:

a = the adhesion between the pile and the soil
σ_n = the normal stress at the interface
δ = the interface friction angle

Based on experience, the interface friction angle between steel and soil is generally assumed to be between 50 and 70 % of the internal friction angle of the specific soil type, and the adhesion between pile and soil about half the cohesion of the soil.
Contact-frictional plane elements were not available in the 3-dimensional configuration within the programme at the time of the analysis. The alternative way, in which the interaction is simulated with elasto-plastic spring elements, would have required an undue amount of effort in a large 3-dimensional model. Furthermore a test run showed that this would reduce the speed of convergence to a non-acceptable level. Thus two extreme cases were considered: a so-called fully bonded and a completely smooth situation. In the first, fully bonded, case no relative displacements between pile and soil were allowed at the interface. In the completely smooth case there was no resistance against shearing at the interface, and in the normal direction there was contact only when the stresses were compressive. Tensile stresses would not be transmitted, in that case there was no contact at the interface (tension cut-off).

6.4 *Finite element model*

During discretization of a physical problem into a computer model one must always consider the working boundary conditions as for instance the available computing power and the accuracy criteria for the elements, depending on the "length-width ratio" of the elements. Furthermore the layered soil profile has to be modelled as correctly as possible. Since the number of data to be processed in a 3-dimensional analysis very easily becomes too big to handle, these aspects become very important and require careful consideration. The mesh used for the final calculations, which is shown on page 49 and in Fig. 6.2 and 6.3, was considered to be the best compromise possible for the given boundary conditions.
Due to symmetry considerations only half of the system was modelled. In the horizon-

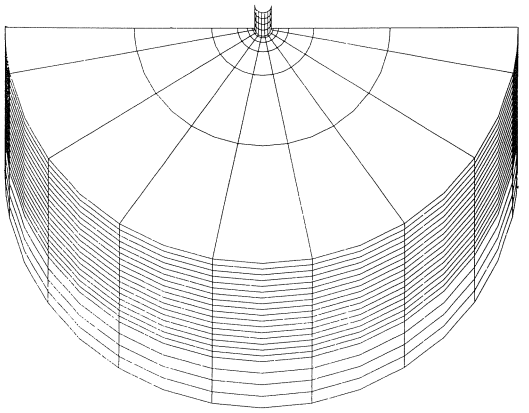

Fig. 6.2 3-dimensional finite element mesh "backside shown from above with half the pile at the background".

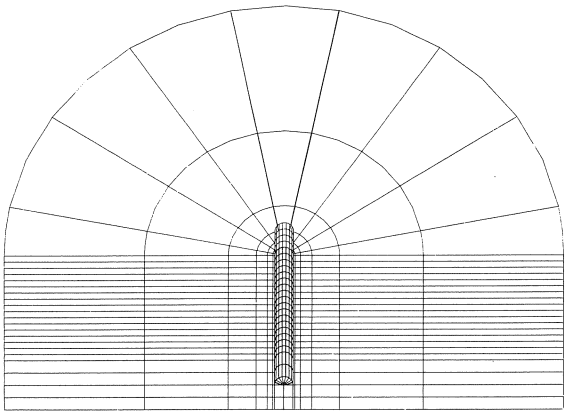

Fig. 6.3 3-dimensional finite element mesh "looking onto the plane of symmetry with half the pile in the center".

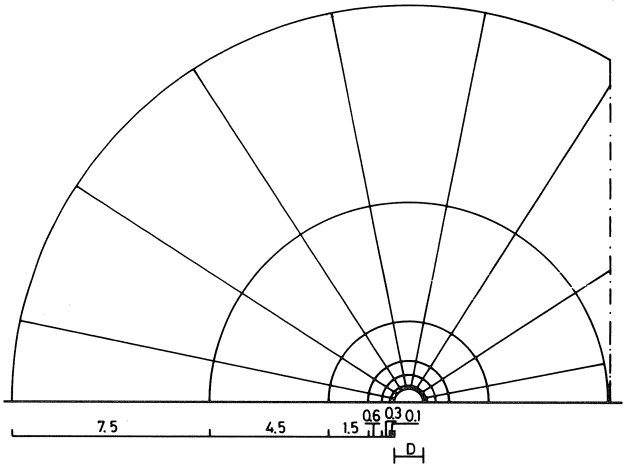

Fig. 6.4 3-dimensional finite element mesh "horizontal plane".

tal plane the mesh was divided into 9 segments, forming a half circular plane with a total radius of 14.5 times the diameter of the pile. Each segment contains 6 elements, the size of which increases with the distance to the pile, see Fig. 6.4. In the vertical plane 21 layers were modelled, 17 of these represent soil layers with a thickness of 0.5 m. The last 4 layers, including 2 positioned beneath the pile tip have thicknesses of 1.0 m.
Due to external complications the 3-D finite element calculations had to be performed after the test. The input however was fully documented before performing the field test, so curve-fitting to the test result was not possible. Because of the computing effort involved it was only possible to analyse three different cases. Starting from a reference case, the influence of two parameters could be studied. The following parameters were chosen for this sensitivity study:
- the roughness at the interface pile-soil;
- the geometry of the steel profiles connected to the pile.

Consequently the influence of a variation of the soil-parameters was not studied. The values used in the calculations were based upon the total soil investigations, and are presented in paragraph 6.5.

The different calculations can be characterized as follows:

Run 1: "rough circular pile"
- the displacements of pile and soil are fully connected in all directions at the interface
- the stiffness of the profiles is added to the shell elements resulting in fictitious values for Young's modulus and the wall-thickness, to model the bending, EI, and normal stiffness, EA, in a correct way.

Run 2: "smooth circular pile"
- the displacements of pile and soil are radially linked in the loading direction
- there is no contact between pile and soil "behind" the pile; this characterizes the gapping-mechanism: no contact under tensile stresses
- in the vertical direction and parallel to the pile-circumference shear stresses cannot be transferred from pile to soil. This implies that the surface is perfectly smooth
- the stiffness of the profiles is added to the shell elements in the same way as in run 1.

Run 3: "rough pile including steel profiles"
- the displacements of pile and soil are connected in all directions at the interface as in run 1
- the geometry and stiffness of the steel profiles are added to the model as indicated in Fig. 6.5. To enable modelling of these steel profiles the size of the first row of elements was chosen such that they could easily be incorporated.

6.5 *Predictions*

6.5.1 Soil parameters, based on soil investigations

The translation of the results of soil investigation tests to material parameters requires

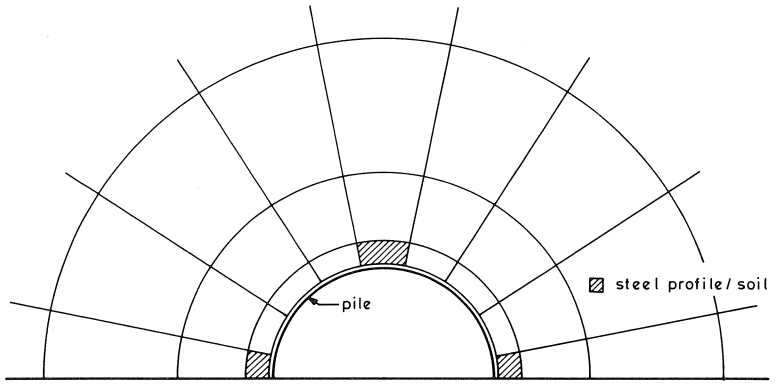

Fig. 6.5 Volume elements representing the steel profiles connected to the test pile.

distinguishing between the undrained behaviour of the soft cohesive soil layers as clay and peat, and the drained behaviour of the granular sandy layers.

a. *Peat and clay layers*
Undrained behaviour implies that the soil behaves like an incompressible medium. For the elastic part of the model this means that the undrained Poisson's ratio, ν_u, will be equal to 0.5 and the undrained bulk modulus, K_u, will be infinite. The undrained shear modulus, G_u, will be approximately equal to the drained modulus, G_d. It can be concluded that the undrained Young's modulus, E_u, is not equal to the drained one. E_u is related to E_d in the following way:

$$E_u = 3\ E_d / 2(1 + \nu_d) \tag{6.6}$$

where ν_d for clay is about 0.2. Additionally, for the plasticity model the undrained shear strength, c_u, is needed.

b. *Sand layers*
To model the mechanical behaviour the following elastic and plastic parameters are needed: drained Young's modulus E_d and drained Poisson's ratio ν_d and the effective angle of internal friction ϕ' and the effective shear strength c'. Since the density of the sand layers can be classified as low to medium dense, the dilatancy angle ψ is chosen equal to zero.

Note: In this chapter the elastic parameters E and G referred to are E_{50}- and G_{50}-values, defining the secant stiffness corresponding to the strain at half the maximum stress level.

6.5.2 Level 1 (CPT's)

The undrained shear strength c_u and the undrained Young's modulus E_u were determined as:

peat: $c_u = 1/20 q_c$ and $E_u = 3.0 q_c$
clay: $c_u = 1/15 q_c$ and $E_u = 7.5 q_c$

For sand the relation between ϕ' and q_c according to l'Herminier (1953) was applied. This method was corrected in such a way, that the lower bound for ϕ' is equal to 30°. The drained Young's modulus E_d was chosen equal to 3.0 times q_c while ν_d was equal to 0.33.
Table 6.1 summarizes the distinguished soil layers and corresponding parameters following from level 1 soil investigations: cone penetration testing. For numerical reasons the upper bound of Poisson's ratio ν is 0.49.

Table 6.1 Material parameters following from cone penetration testing

layer no	depth [m]	ϱ [ton/m^3]	E [kN/m^2]	ν [–]	ϕ' [°]	c' [kN/m^2]	c_u [kN/m^2]
1:	This layer is absent due to excavation						
2:	1.5 to 2.5	1.60	2250	0.49	-	-	20.0
3:	2.5 to 3.5	1.10	1200	0.49	-	-	20.0
4:	3.5 to 4.1	1.50	2250	0.49	-	-	20.0
5:	4.1 to 4.6	1.10	1200	0.49	-	-	20.0
6:	4.6 to 6.4	1.50	2250	0.49	-	-	20.0
7:	6.4 to 6.8	1.10	1350	0.49	-	-	25.0
8:	6.8 to 7.0	1.10	3000	0.49	-	-	25.0
9:	7.0 to 7.3	1.50	1500	0.49	-	-	25.0
10:	7.3 to 8.0	1.10	3750	0.49	-	-	30.0
11:	8.0 to 11.0	1.90	3600	0.33	30.0	0.0	-
12:	11.0 to 12.3	2.00	10500	0.33	32.5	0.0	-
13:	12.3 to 13.6	1.95	4500	0.33	30.0	0.0	-
14:	13.6 to 15.0	1.60	5200	0.49	-	-	60.0

- : not applicable

Table 6.2 Material parameters following from the laboratory tests performed on the undisturbed samples

layer no	depth [m]	ϱ [ton/m^3]	E [kN/m^2]	ν [–]	ϕ' [°]	c' [kN/m^2]	c_u [kN/m^2]
1:	This layer is absent due to excavation						
2:	1.5 to 2.5	1.50	4500	-	-	-	18.0
3:	2.5 to 3.5	1.05	2400	-	-	-	19.5
4:	3.5 to 4.0	1.40	-	-	-	-	-
5:	4.0 to 8.0	1.50	6250	-	-	-	21.0
6:	8.0 to 11.0	1.80	-	-	-	-	-
7:	11.0 to 12.5	1.80	-	-	-	-	-
8:	12.5 to 14.2	1.70	-	-	-	-	-

- : not tested

6.5.3 Level 2 (boring and laboratory tests)

The empirical relations between the plasticity index and the undrained shear strength and the shear modulus, equations (5.2) and (5.3), were used. It should be pointed out

that the shear modulus resulting from the plasticity index has a larger value than the one according to triaxial and simple shear testing, whereas the undrained shear strength has a lower value. This clearly shows that one must be careful in using empirical relations; it is very important to be aware of the basic ideas or circumstances of the relation.

6.5.4 Level 3 (pressuremeter tests)

According to the methods described in section 3.4 the results of the retrojet pressuremeter tests were used to derive the undrained shear strength and Young's modulus of the soft soil layers.
This results in the following table of mechanical properties for the soft soil layers.

Table 6.3 Material parameters following from pressuremeter tests

depth [m]	σ_η [kN/m^2]	G [kN/m^2]	c_u [kN/m^2]
1.80	27	600	27.7
2.90	36	1100	23.5
3.80	45	1450	22.2
4.50	50	1450	17.5
5.40	56	1150	27.2
6.40	66	2300	25.2
7.30	72	3050	39.9
8.00	78	750	50.6

6.5.5 Final choice of parameters

Based upon the complete soil investigations the following layers and corresponding parameters were used as best estimate and input for the 3-dimensional finite element calculations:

Table 6.4 Soil layers and material parameters used in the 3-dimensional finite element analyses

layer no	depth [m]	ϱ [ton/m^3]	E [kN/m^2]	ν [–]	ϕ' [°]	c' [kN/m^2]	c_u [kN/m^2]
1:	This layer is absent due to excavation						
2:	1.5 to 2.5	1.50	4500	0.49	-	-	18.0
3:	2.5 to 3.5	1.05	2400	0.49	-	-	19.5
4:	3.5 to 4.0	1.40	4500	0.49	-	-	18.0
5:	4.0 to 8.0	1.50	6250	0.49	-	-	21.0
6:	8.0 to 11.0	1.80	3600	0.33	30.0	0.0	-
7:	11.0 to 12.5	1.80	10500	0.33	32.5	0.0	-
8:	12.5 to 14.0	1.70	4500	0.33	30.0	0.0	-
9:	14.0 to 15.0	1.60	5200	0.49	-	-	60.0

- : not applicable

6.6 *Loading, numerical procedure*

As mentioned before, three calculations were performed: (1) rough circular pile, (2) smooth circular pile and (3) rough pile including steel profiles. The load was applied as a prescribed displacement at the top of the pile. Displacement increments of 20 or 10 mm were introduced. A constant stiffness iteration procedure was used. The adopted convergence tolerance was 1.0 percent.
Some statistical values: the total finite element model consisted of 20.578 degrees of freedom and half the bandwidth of the system matrix to be solved was 1331. Each complete calculation required a computing (CPU) time of about 10 hours on the Convex-C201 mini computer system of TNO-BOUW.

6.7 *Results*

Using the finite element method a linear elastic calculation must be performed prior to an elasto-plastic calculation. The results of the linear elastic calculations were visualized using PATRAN, and are shown in the coloured figures (pages 49, 52, 53, 56, 57, 60, 61, 64) for run 3. The Von Mises stress σ_{eq} presented in one of the figures is defined as:

$$\sigma_{eq} = (\sigma_{xx}^2 + \sigma_{yy}^2 + \sigma_{zz}^2 + \sigma_{xx}\sigma_{yy} + \sigma_{yy}\sigma_{zz} + \sigma_{zz}\sigma_{xx} + 3(\sigma_{xy}^2 + \sigma_{yz}^2 + \sigma_{zx}^2))^{0.5} \qquad (6.7)$$

At the moment of analysis results of nonlinear, elasto-plastic analyses could only be visualized 2-dimensionally. These results are presented below. Comparing these ways of presentation clearly shows the advantages of 3-dimensional colour graphics.
The relation between the pile-top displacement and the calculated total horizontal reaction force is presented in Fig. 6.6. It can be seen that there is a significant difference between the completely smooth and the fully rough approach. This indicates that modelling the interface behaviour in a correct way is very important.

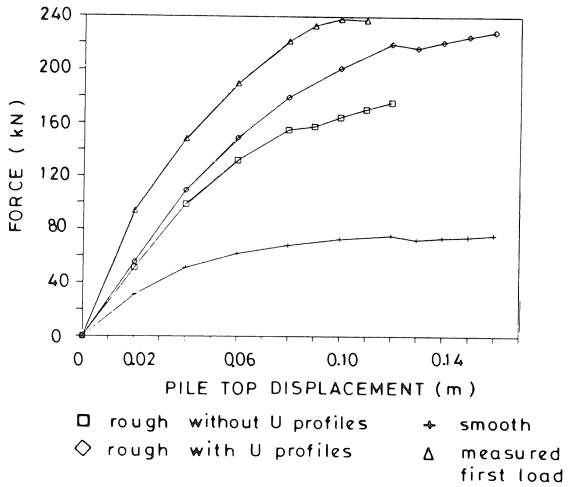

Fig. 6.6 Load-displacement curves from 3-dimensional finite element calculations.

The influence of the geometry of the steel profiles connected to the pile can also be observed: with increasing deformation the profiles add a significant stiffness and strength to the pile behaviour. The dip appearing in all three curves is a result of decreasing the step-size from 20 to 10 mm and therefore a numerical effect only.
The deformation of the pile and the surrounding soil is presented in Fig. 6.7 and 6.8. In

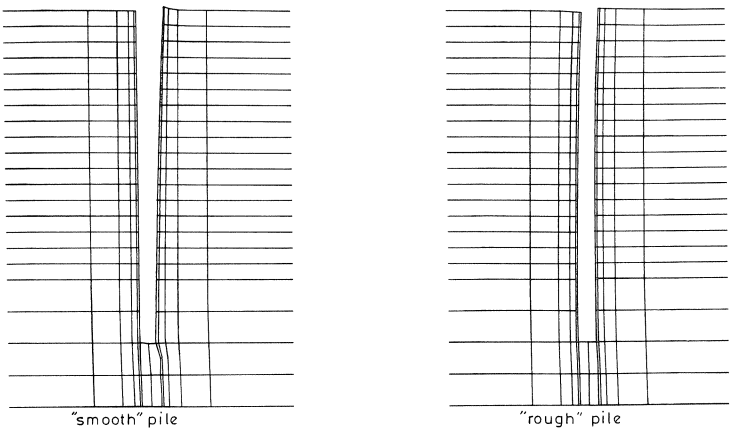

Fig. 6.7 Deformation of the soil, in vertical plane, for a pile-top displacement of 100 mm; smooth pile (a) and rough pile (b).

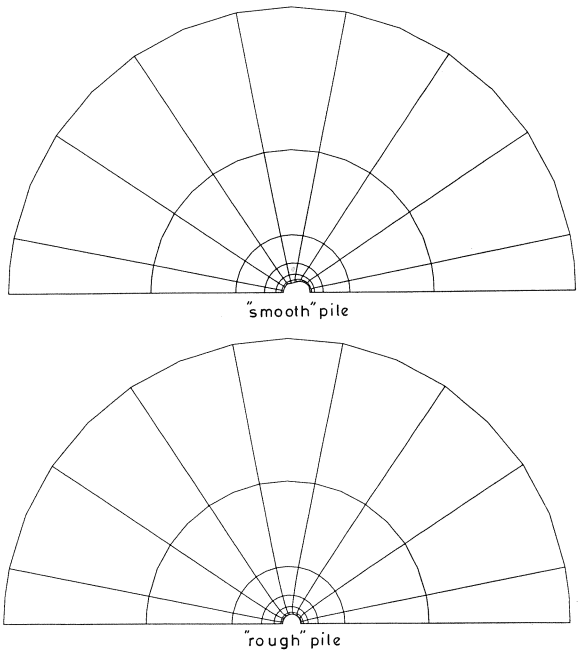

Fig. 6.8 Deformation of the soil, in horizontal plane, for a pile-top displacement of 100 mm; smooth pile (a) and rough pile (b).

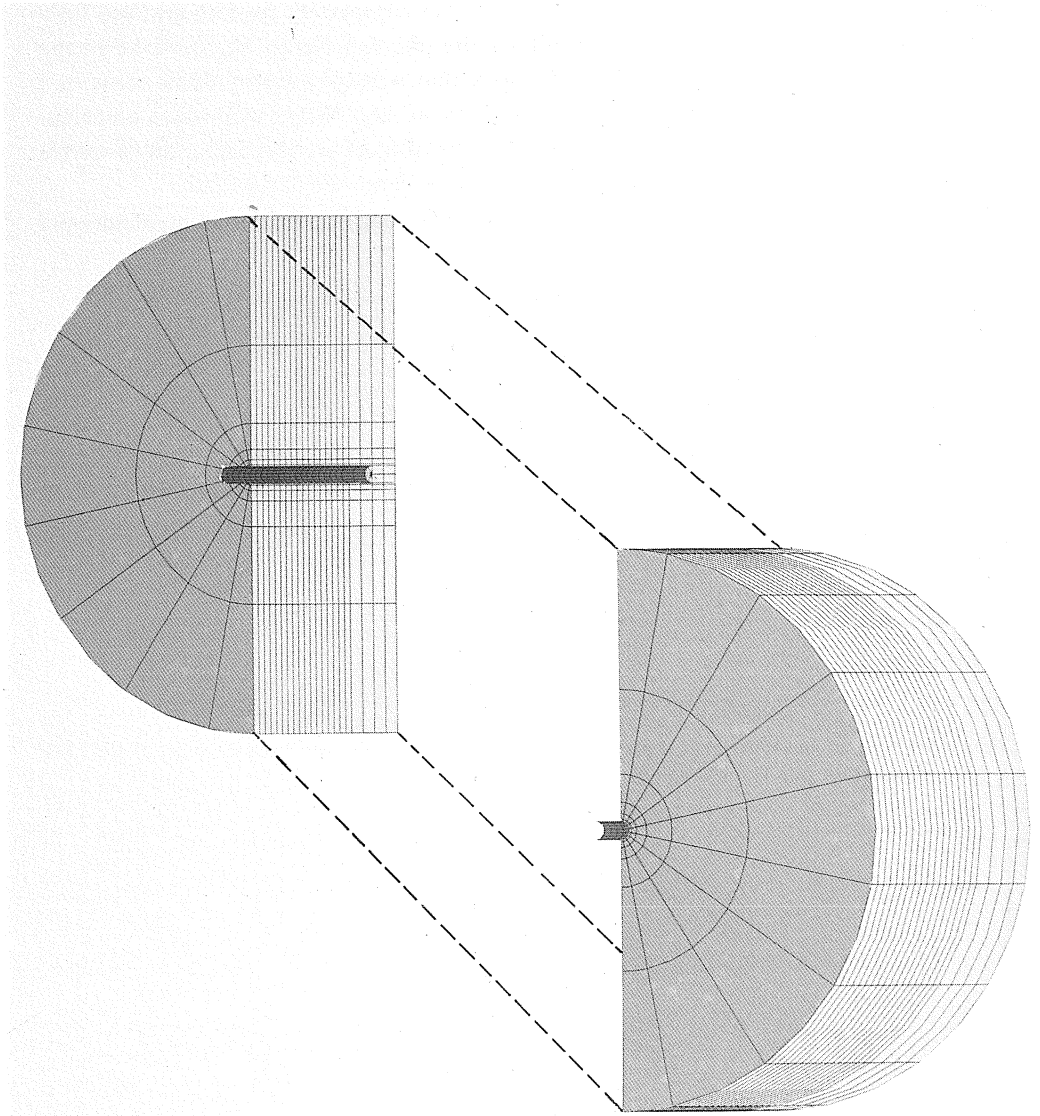

Finite element model of pile and soil.

these figures the deformation is compared for the completely smooth and the fully rough case without profiles. The gap behind the pile can clearly be observed in the smooth situation. Furthermore it can be seen that vertical deformations occur in a small zone in front of the pile, especially near the surface. When comparing all calculated results it shows that the incremental deformation in vertical direction increases relatively when compared to the horizontal one, at large displacements.
Fig. 6.9 and 6.10 show soil stresses around the pile due to horizontal loading. Relatively

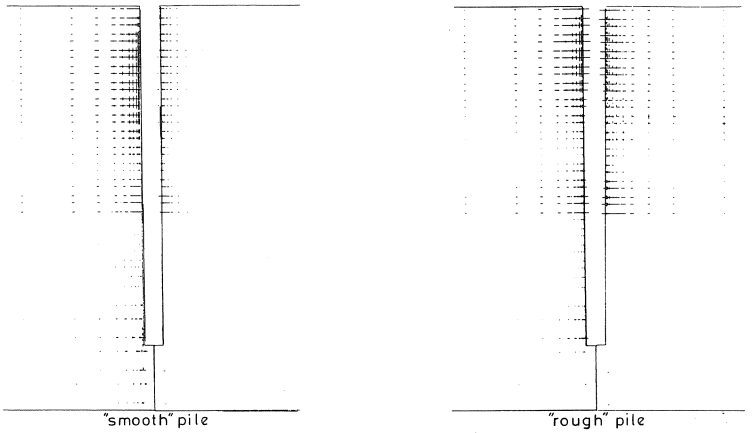

Fig. 6.9 Soil-stresses, in vertical plane, of pile and soil for a pile-top displacement of 100 mm; smooth pile (a) and rough pile (b).

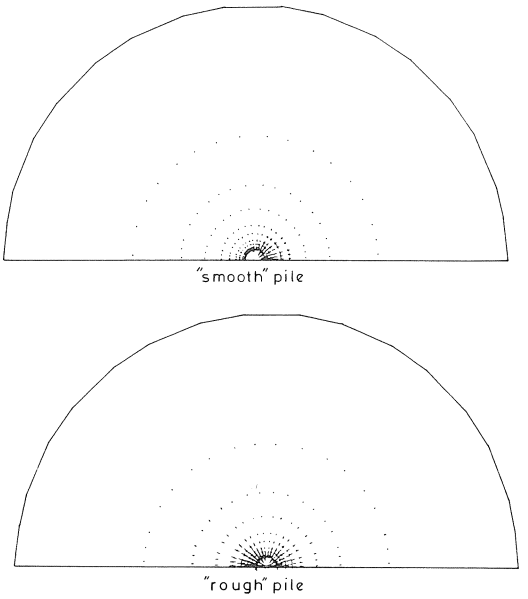

Fig. 6.10 Soil-stresses, in horizontal plane, of pile and soil for a pile-top displacement of 100 mm; smooth pile (a) and rough pile (b).

stiff layers can be recognized as regions with stress concentrations. Like the deformation the stresses are also concentrated in a small zone around the pile top. Based on these figures it can be concluded that the induced vertical stresses due to the horizontal deformation of the pile are about 30 % of the horizontal ones. It appears that especially in the upper layers, the vertical stress component cannot always be neglected for horizontal loading. This is in accordance with observations of Matlock (1970).
The bending moment in the pile as a function of depth, for a rough pile, is presented in Fig. 6.11. With increasing load level, the depth at which the maximum bending moment occurs moves downward. Along the whole length of the pile the bending moment in the pile has the same sign. The shape of the lines presented is not very smooth, the effect of the increase of the bending stiffness at a distance of 2 m from the pile top, caused by the steel profiles, is clearly visible. The irregular shape is caused by discontinuities in the calculated stresses, and has no physical relevance.
To conclude, the results presented clearly indicate that it is very important to model the interface, both the frictional and the gapping, mechanism between pile and soil in a correct way. The range for the horizontal force at the same pile top displacement resulting from the limit cases, run 1 "rough circular pile without the gapping mechanism" and run 2 "smooth circular pile" is a factor between 2 and 3, depending on the load level.

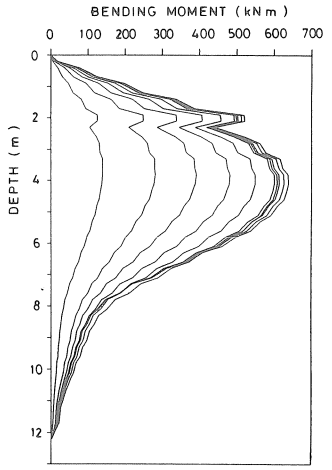

Fig. 6.11 Bending moments in the pile for a number of horizontal force levels; for a rough pile.

7 Full scale field test

7.1 *Test setup*

The test was performed on a previously installed hollow steel pile with a diameter of 0.61 m, a wall thickness of 8.8 mm and a length of 12.5 m. The pile was instrumented with 40 strain gauges, distributed, in axial direction, in 4 rows of 10 gauges each at 0°, 90°, 180° and 270° positions. The strain gauges were covered by steel U-profiles that

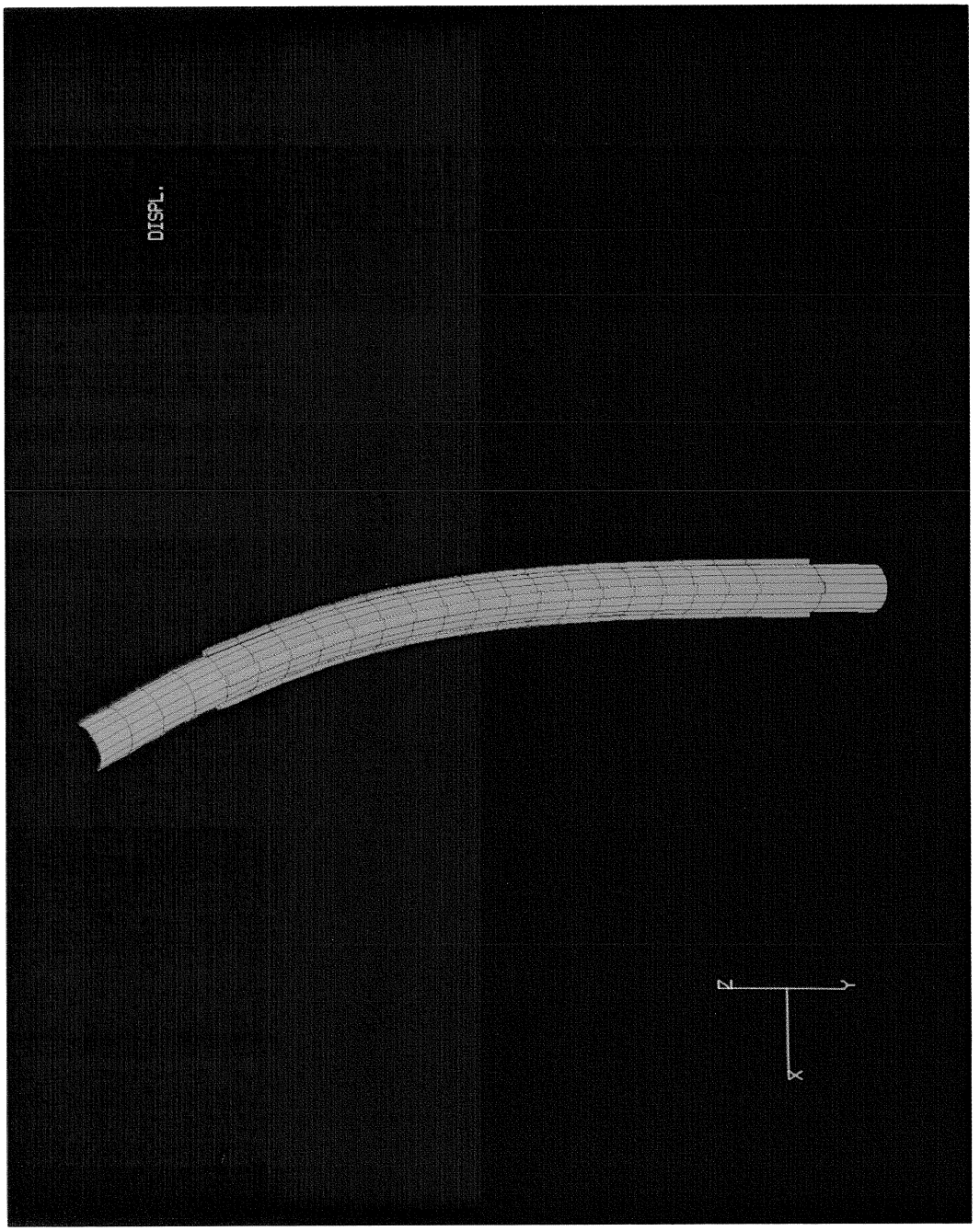

Deformed pile model, consisting of shell elements and volume elements representing the steel U profiles.

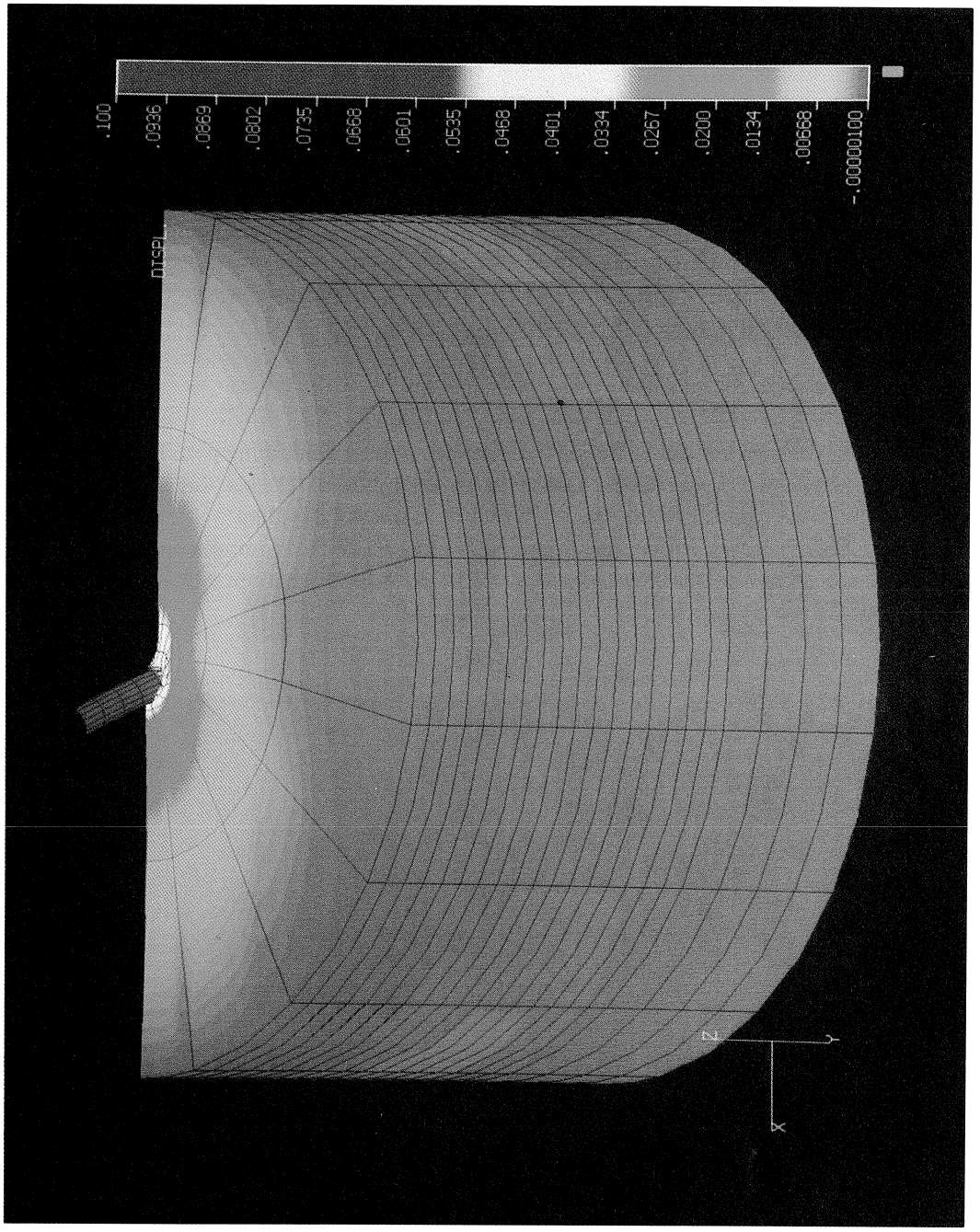

Calculated displacement distribution for a prescribed pile top displacement of 0.1 m.

were welded to the outer pile surface for protection during pile driving. The test set up is shown in Fig. 7.1. A jack with an ultimate force of 250 kN and a maximum deflection of 150 mm was used to apply the horizontal force at the pile top. The reaction force was generated by a deadmans bed at sufficient distance, 11.5 times the pile diameter, from the pile location. The force acting at the pile top was measured with a load cell placed between the jack and the pile top. This ensured that the force recordings would not be influenced by frictional effects or displacements of the loading system.
In order to eliminate the influence of the top soil fill layer, the mechanical characteristics of which are unpredictable since they strongly depend upon the actual moisture content, this top layer was removed to a depth of 1.5 m around the piletop. The total area of excavation around the pile was 2.6 x 2.6 m^2.

7.2 *Loading scheme*

The loading scheme can be divided into a static and an alternating part. First a quasi-static, sine shaped, one sided, load with an amplitude of 235 kN was applied in 20 seconds. After that three series of alternating loads were applied:

- 10 loading cycles, with a maximum load of 140 kN and a 10 minute pause between each load cycle. This pause was included to allow for dissipation of generated pore-water pressures;

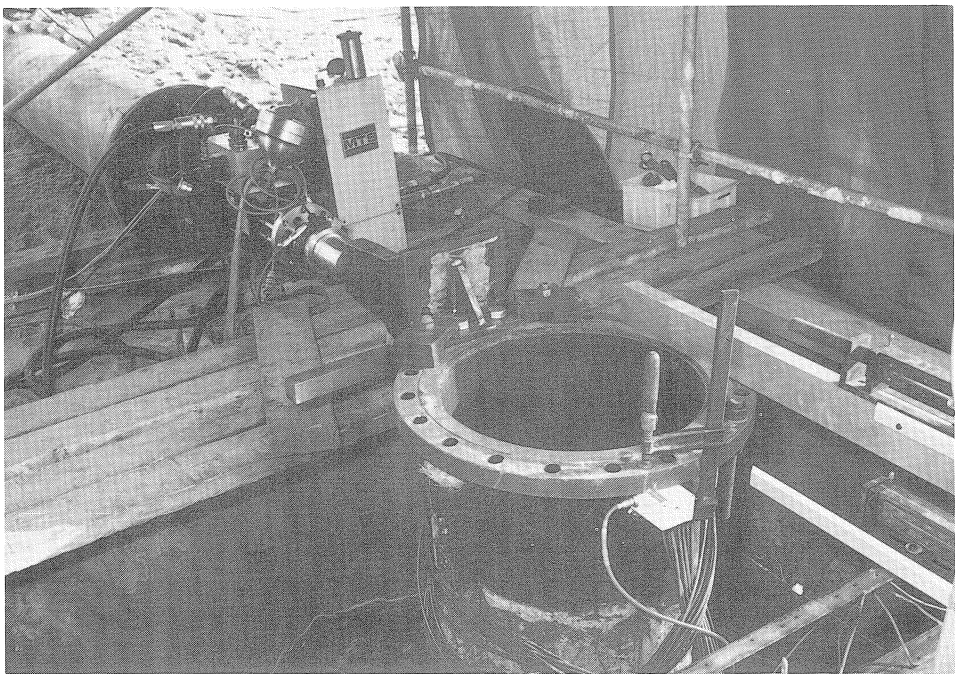

Fig. 7.1 Test setup.

- 30 loading cycles, with a maximum load of 140 kN, without pauses;
- 30 loading cycles, with a maximum load of 172 kN, without pauses.

All these alternating loads were sine shaped, one sided, loadings with a loading time of 9 seconds.
Finally a quasi-static load analoge to the first load was applied, but with a maximum load level of 210 kN.

7.3 *Measurements*

The following data were recorded during the test with a sampling frequency of 5 Hz:
- the horizontal pile top loading force;
- the horizontal pile top displacement;
- the horizontal displacement 1 m below the pile top;
- the steel-strains in 34 strain gauges.

Opening and closure of the gap was visually followed during the tests.
After the tests the final gap width at the backside of the pile was measured.

7.4 *Results*

Results of the tests were gathered in the following groups:
- force-time graphs;
- displacement-time graphs;
- strain-time measurements;
- gap width at the end of the test.

By combining force-time and displacement-time curves, force-displacement graphs were obtained. These curves were derived for all loading cycles. Fig. 7.2, 7.3, 7.4 and 7.5 show the force-displacement curves for the first quasi-static loading, the 10 loading cycles with a 10 minute pause between each cycle, and the 2 x 30 cycles without pauses. Fig. 7.6 shows the extracted results of both the first and the last quasi-static loading. These graphs clearly show that the stiffness of the system is degradated due to cyclic loading. The degradation is largest after the first loading. Further loading cycles show only moderate further degradation.

7.5 *Data reduction*

7.5.1 Bending moments

Using elementary beam theory the bending moments in the pile, and the resulting soil pressures acting on the pile, can be derived from the strains measured with the gauges. Starting with strains measured at two corresponding opposite sides of the pile, ε_1 at one side and ε_2 at the other, the bending moment, M, and the normal force, N, can be derived in a rather straightforward way:

$$M = EI\,(\varepsilon_1 - \varepsilon_2) \,/\, D \tag{7.1}$$

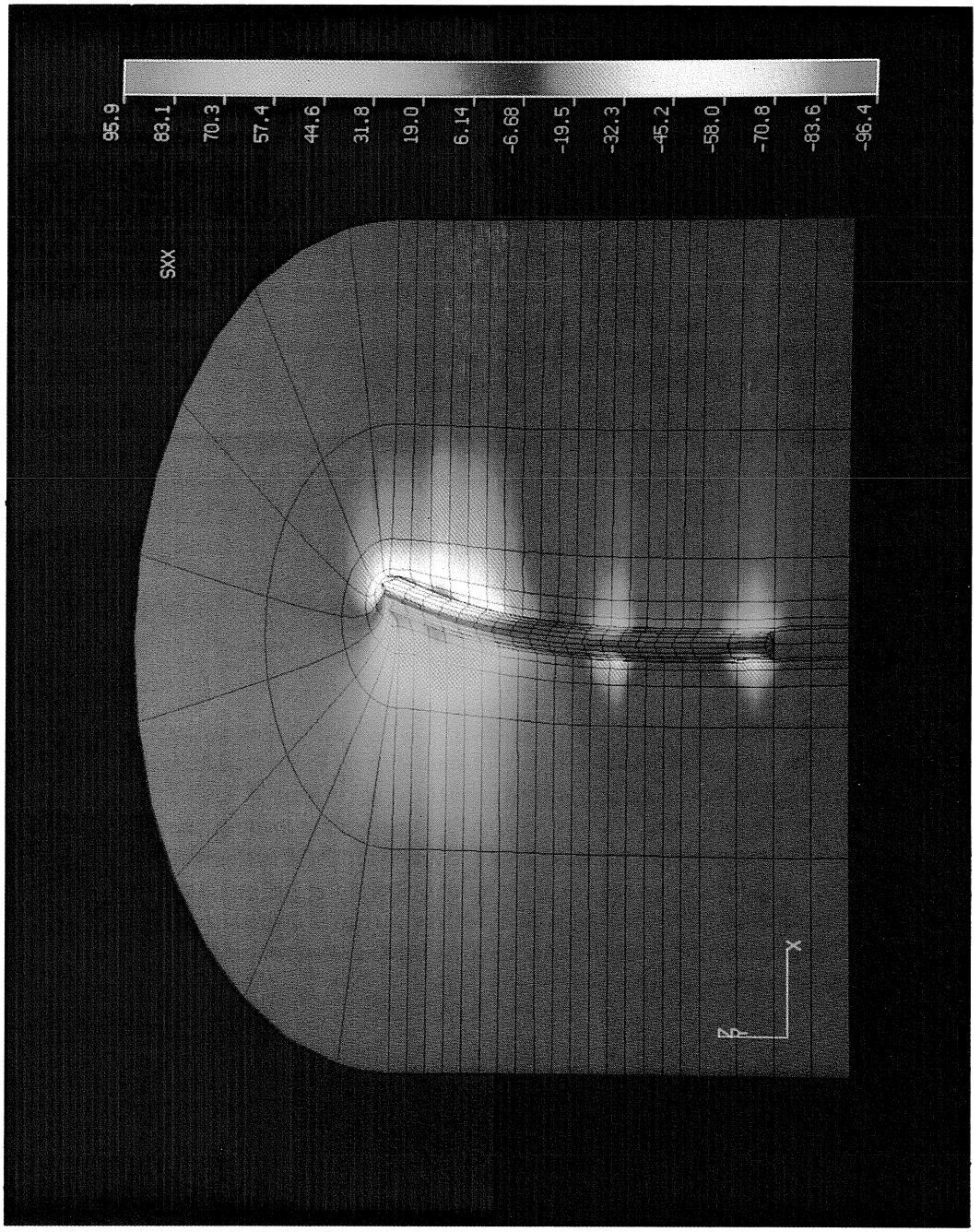

Horizontal soil tresses, σ_{xx}, for a prescribed pile top displacement of 0.1 m.

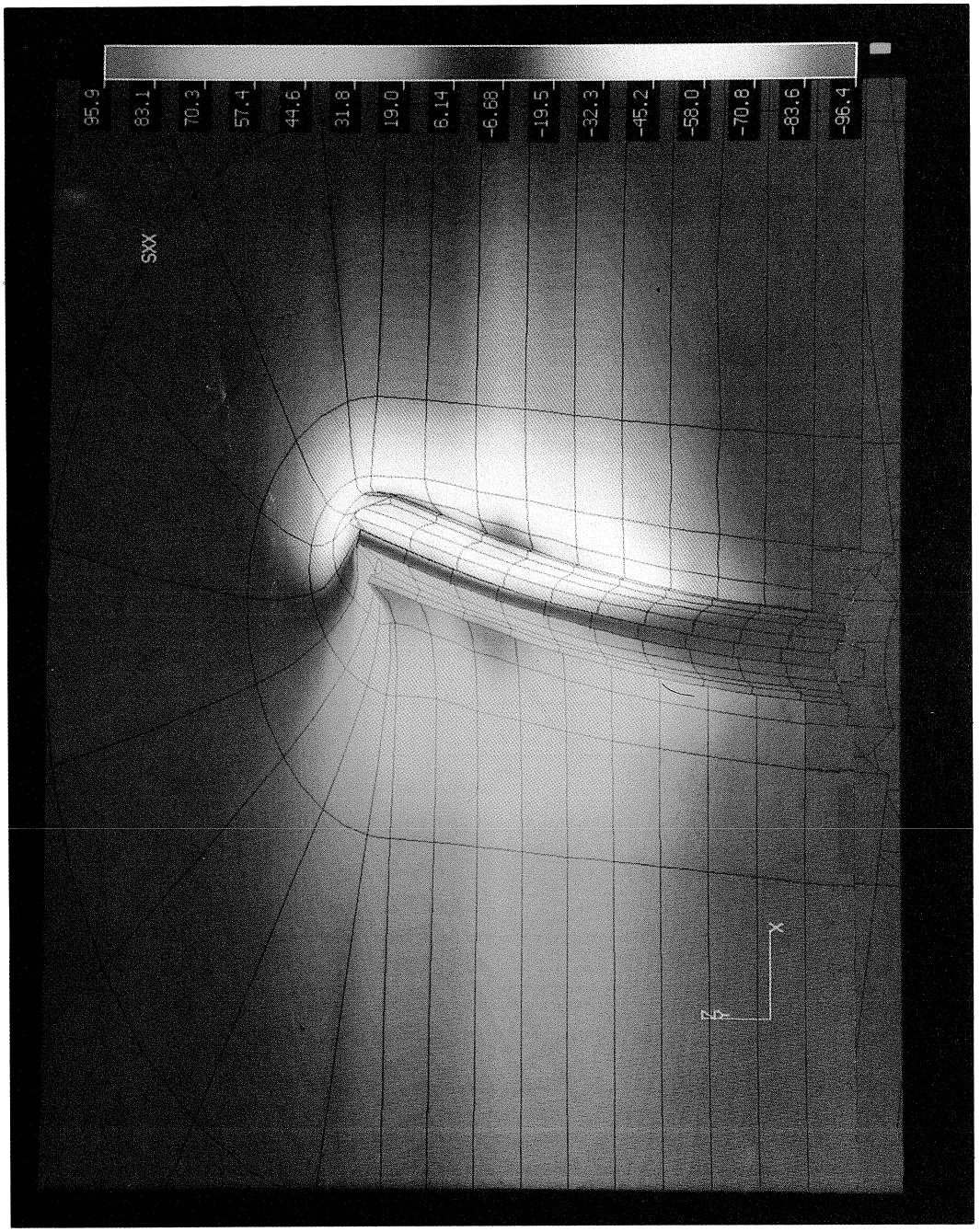

Close-up of the region around the pile top: horizontal soil stresses, σ_{xx}, for a prescribed pile top displacement of 0.1 m.

$$N = EA\ (\varepsilon_1 + \varepsilon_2)\,/\,2 \tag{7.2}$$

where:

EI = the flexural stiffness of the pile
EA = the normal stiffness of the pile
D = the diameter of the pile

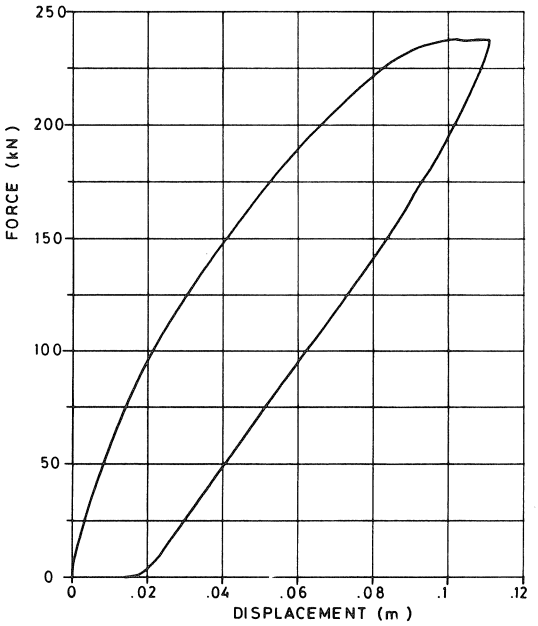

Fig. 7.2 Load-displacement curves for the first quasi-static loading.

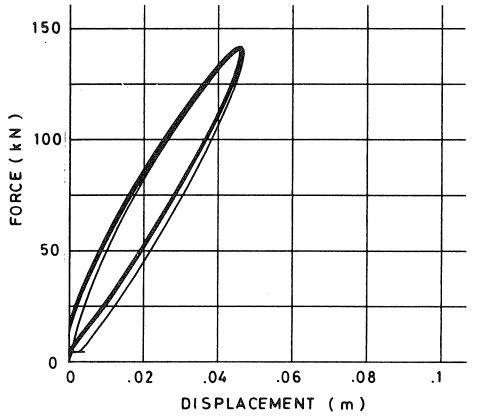

Fig. 7.3 Load-displacement curves for 10 load variations with a maximum load of 140 kN, and a 10 minutes pause between each cycle.

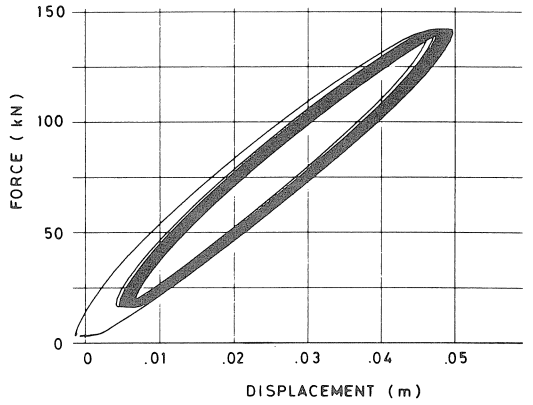

Fig. 7.4 Load-displacement curves for 30 load variations with a maximum load of 140 kN, without pauses.

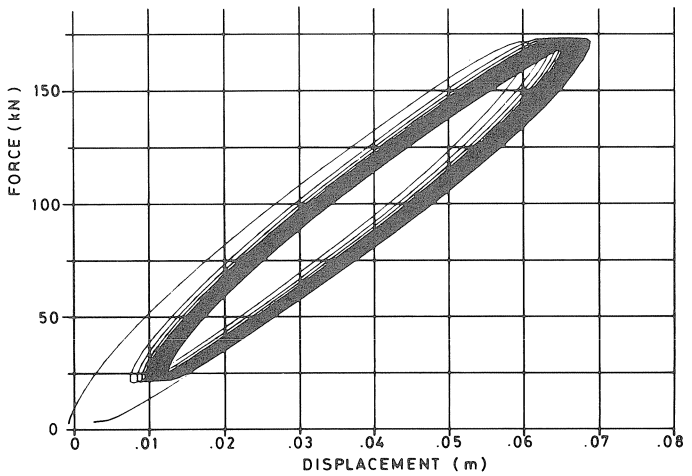

Fig. 7.5 Load-displacement curves for 30 load variations with a maximum load of 172 kN, without pauses.

Fig. 7.7 shows the results for the first loading.

The graphs show that the maximum bending moment occurs at larger depths with increasing loads. It further shows that for relatively small loads a small negative bending moment occurs, indicating that the pile is completely embedded for these cases.

Since the bending moments are derived from the strains measured by the gauges the values obtained include a certain systematic measuring error. An estimate of the error involved can be obtained by comparing the bending moments, at ground surface level,

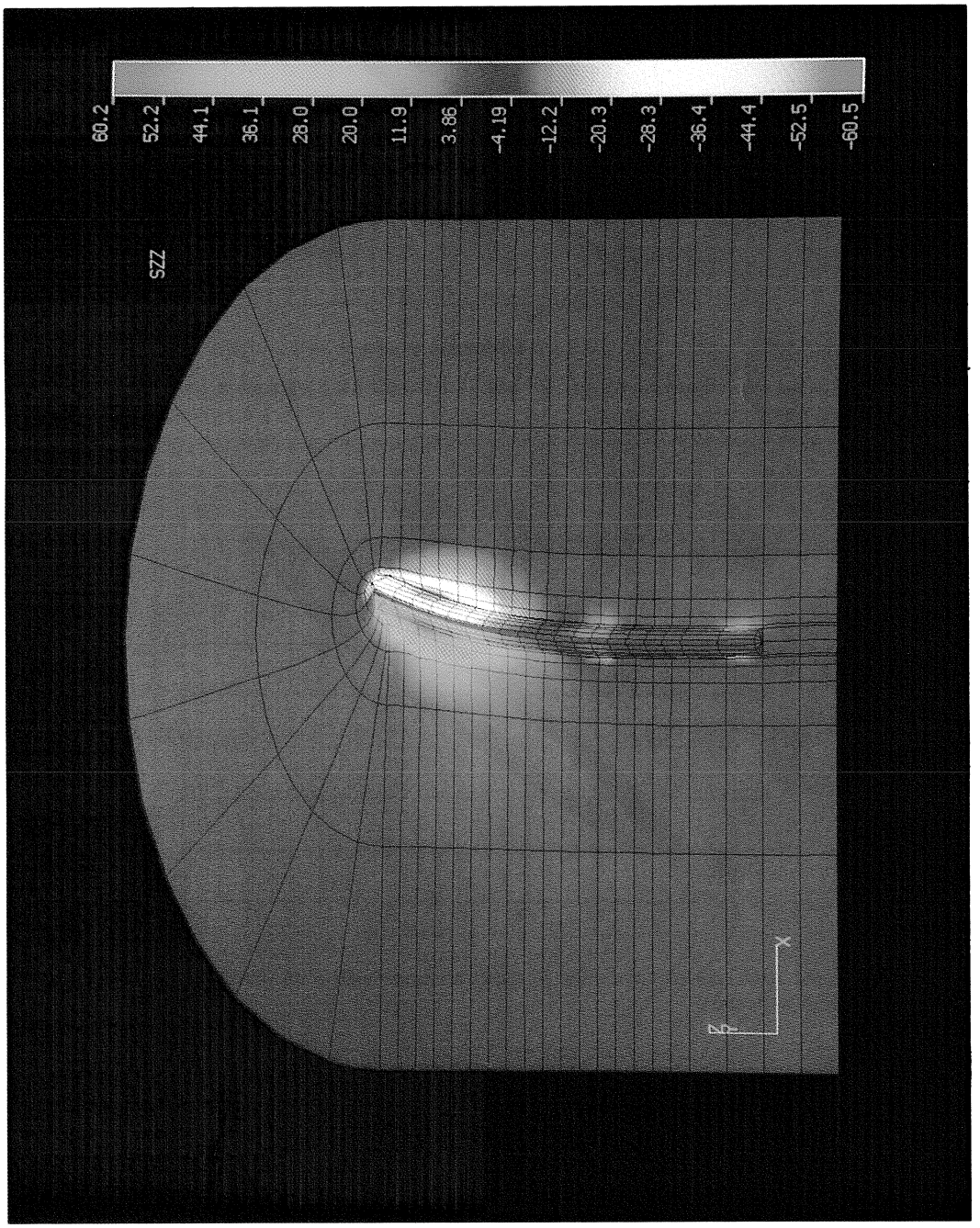

Vertical soil stresses, σ_{zz}, for a prescribed pile top displacement of 0.1 m.

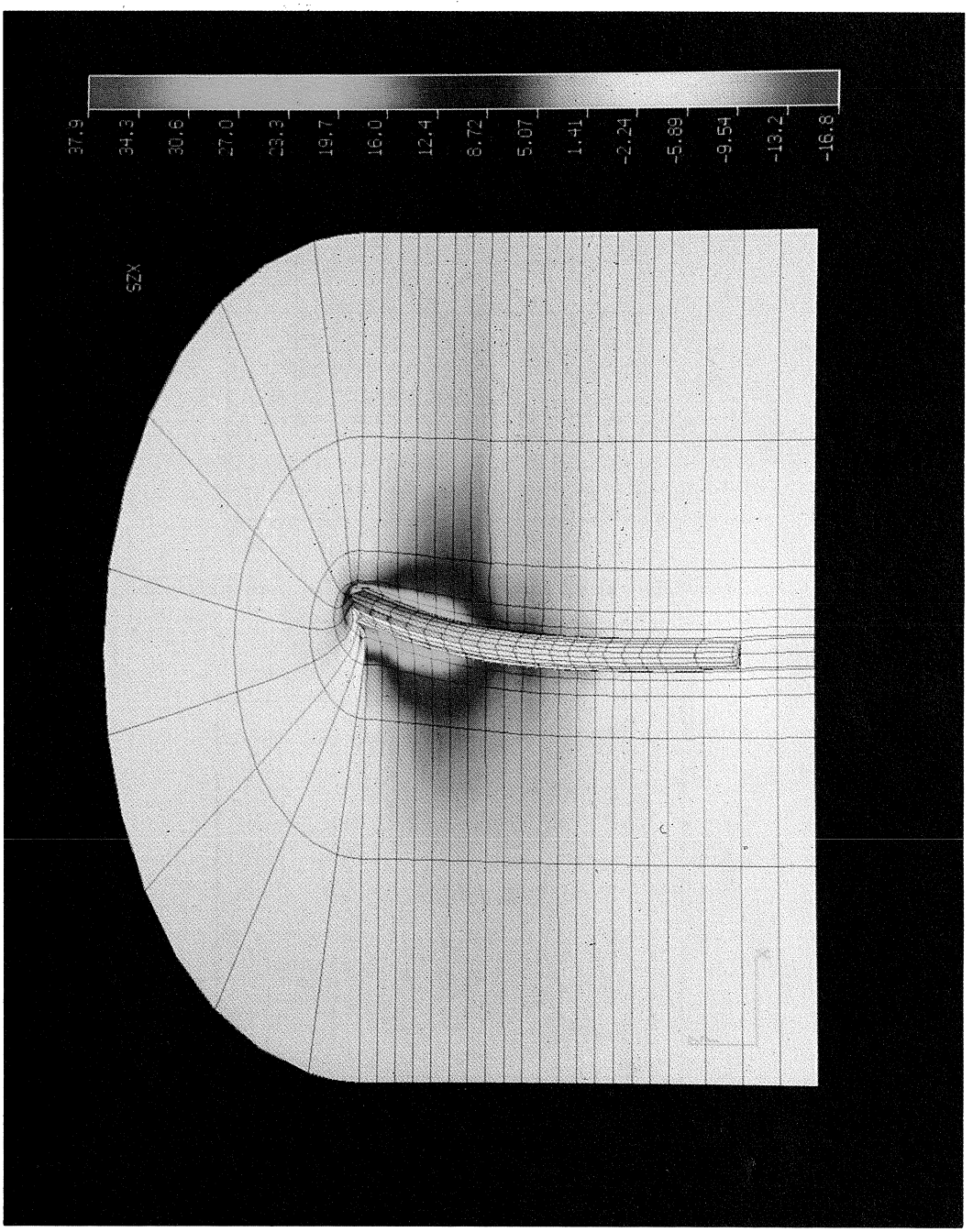

Shear stresses in the soil, σ_{zx}, for a prescribed pile top displacement of 0.1 m.

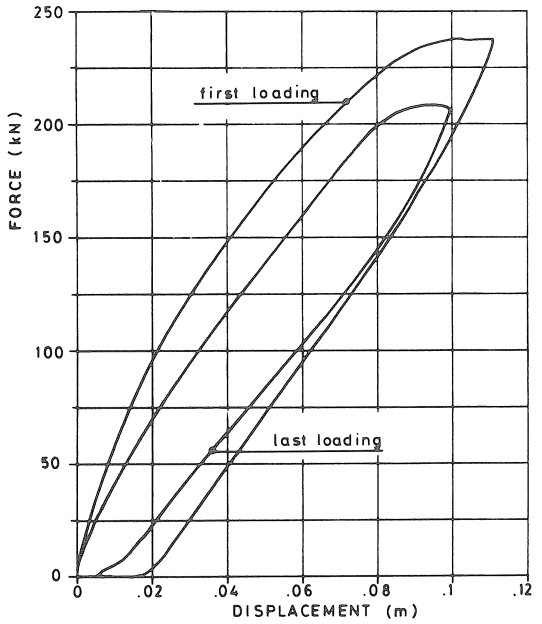

Fig. 7.6 Load-displacement curves for the first and last quasi-static loading.

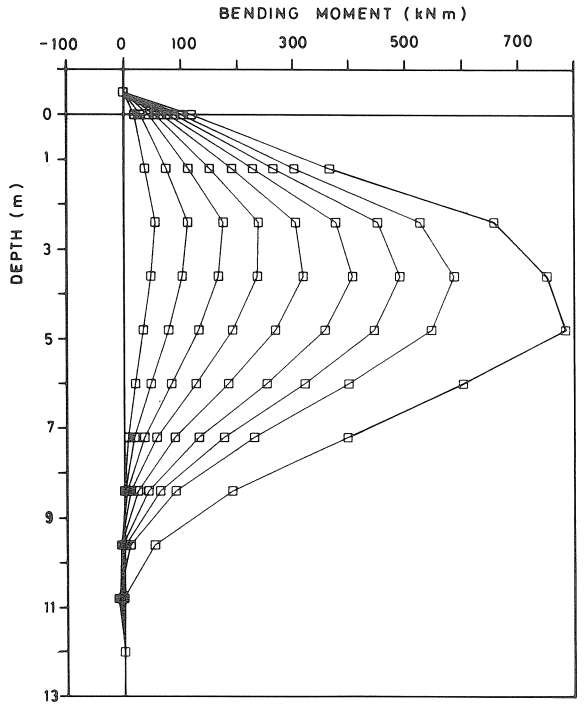

Fig. 7.7 Bending moments as a function of depth for a horizontal load of 25, 50, 75, 100, 125, 150, 175, 200 and 238 kN respectively.

derived from the measured strains with the theoretical values: force multiplied by the working length.
Although every strain gauge has been corrected for its own offset the results show a difference up to about 10 % !

Force at pile top	Depth below the pile top	Bending moments (kNm)		
		theoretical	measured	difference (%)
200 kN	0.5 m	100	101	+ 1
200 kN	1.7 m	340	303	−11
238 kN	0.5 m	119	119	0
238 kN	1.7 m	405	366	−10

After completion of the last loading cycle a last reading was taken to establish the permanent bending moments in the pile after the test. Although some points of the graph shown in Fig. 7.8 cannot be explained it is clear that a considerable bending moment is still present in the pile.

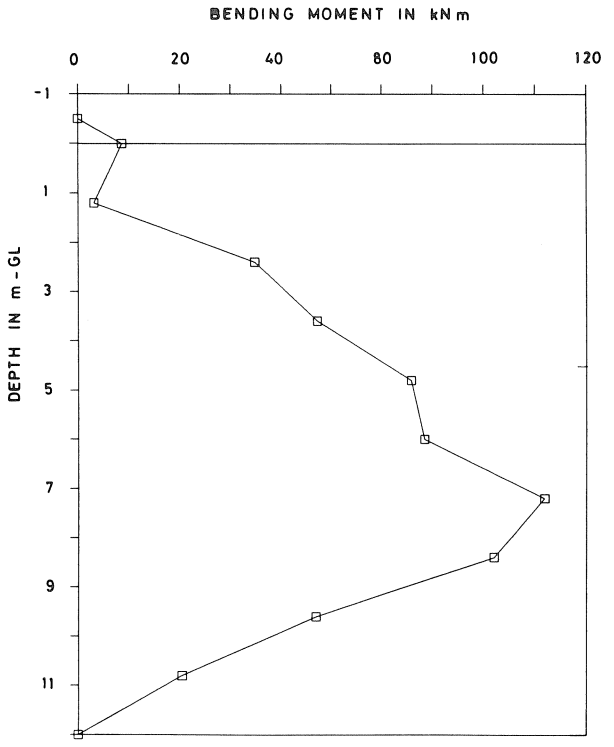

Fig. 7.8 Remaining bending moments in the test pile after the test.

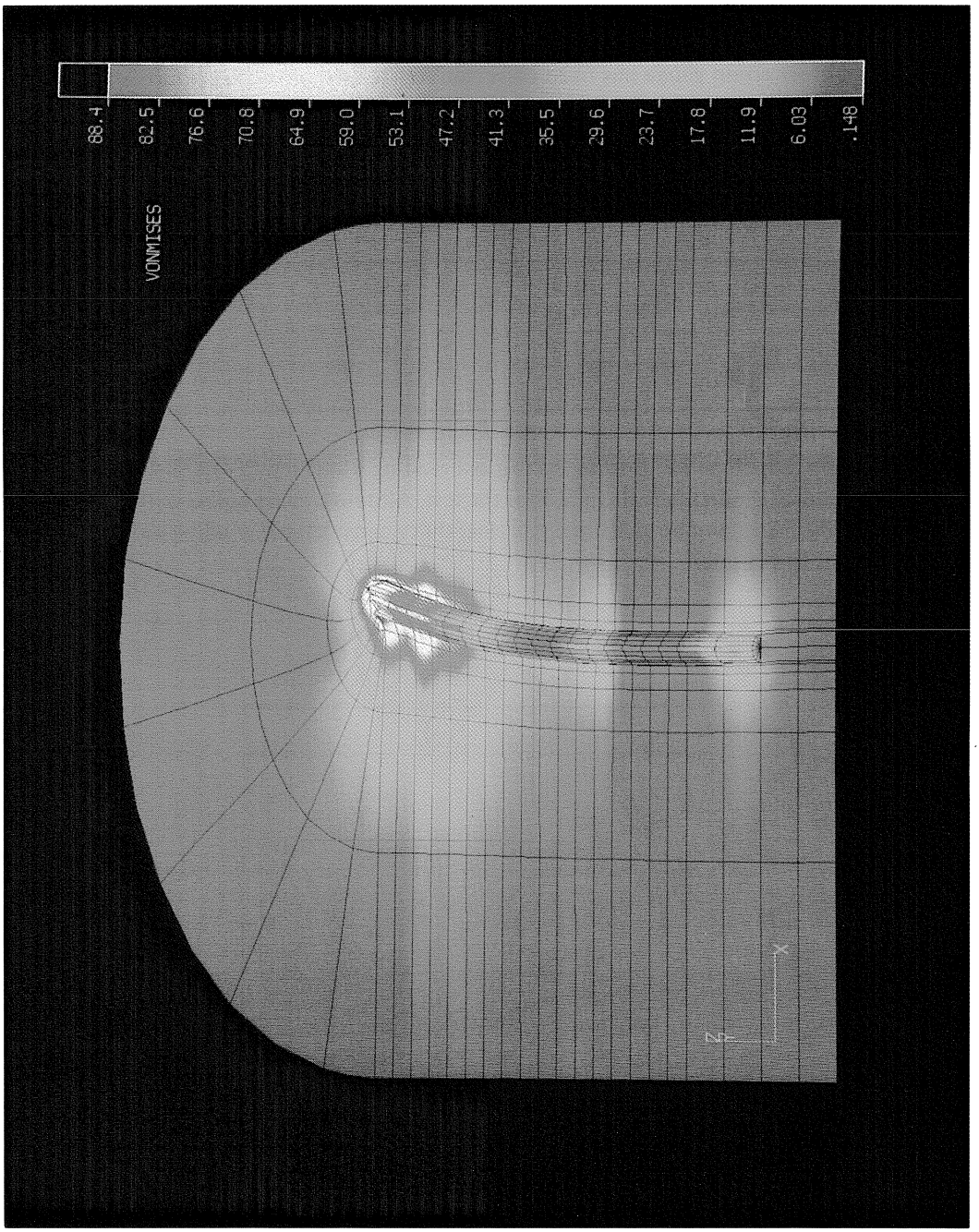

"Von Mises stresses" in the soil for a prescribed pile top displacement of 0.1 m.

7.5.2 Soil pressures

Again using beam theory soil pressures can theoretically be obtained from the bending moments using the second derivative of the bending moments. However, in order to obtain a second derivative the measured bending moments have to be described using a function that can be differentiated at least twice. A common choice is a polynominal of the nth degree, where n varies between 3 and 10. Usually an error estimate of the resulting soil pressures is not included in the procedure.

The method used in this project is similar to the one decribed above, however in this case an error estimate is included. A computer programme developed by Delft Geotechnics (Calle,1979) was applied. In this programme the pile can be divided into 10 sections. Each section has its own polynominal. This enables derivation of soil pressures that are discontinuous at a boundary of soil layers. A restriction of the programme is that the order of the polynominals has to be the same for all sections.
Performing analyses using different orders of the polynominals leads to the following conclusions:

1. The free protruding end of the pile can not be described correctly in this manner.
2. The results strongly depend upon the degree of polynominal chosen. Higher order polynominals tend to render excessive pressures near the borders of the domain. Addition of known data, for example the size of the bending moment at the ground surface and pile tip level does not have a positive influence on these results. Therefore high degree polynominals are not suited for this type of analyses. Some results are shown in Fig. 7.9.

These results show that the choice of the degree of the polynominal defines the shape and magnitude of the calculated soil pressure distribution along the pile. Since the

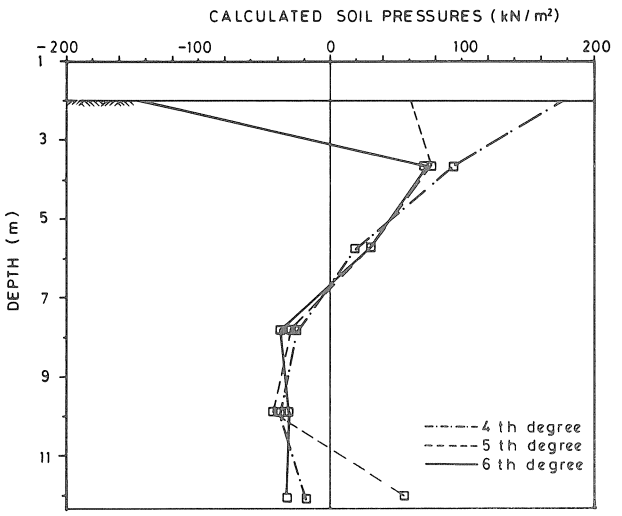

Fig. 7.9 Soil pressures derived from strains by polynominal analyses.

a)

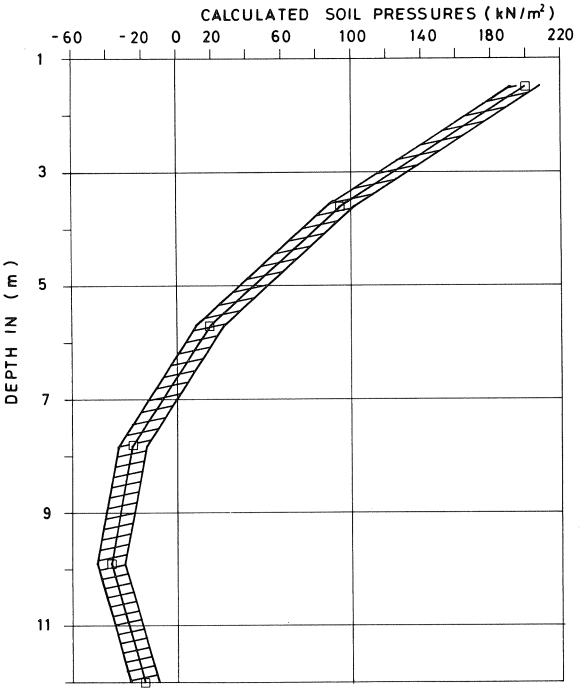

b)

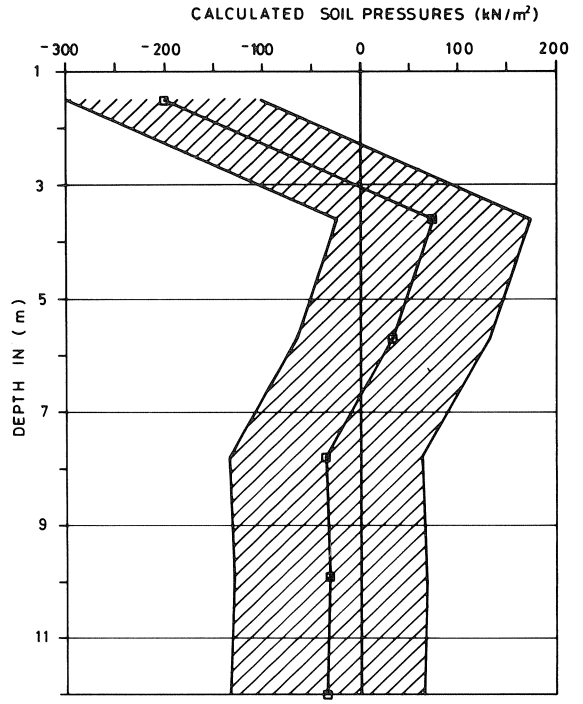

Fig. 7.10 95 % confidence belt of derived soil pressures for a 4th (a) and a 6th (b) order polynominal.

shear force in the pile is known for the protruding part of the pile this value can be used for an error estimation. Comparison of the values obtained from the polynominals with the theoretical value renders a 5th degree function as being the best fit.
However, when the effects of errors in the bending moments are taken into account, reliability is reduced considerably. In that case the soil pressures have to be regarded as values that can vary with a certain deviation. This deviation depends on both the error in the bending moments and the degree of the polynominal. Fig. 7.10 shows a 95 % confidence belt for both a 4th and a 6th degree polynominal based on a 1 % error in the bending moments. The results clearly show that higher order polynominals render larger uncertainties in the calculated soil pressures.

7.5.3 Energy dissipation

In order to describe loss of energy during loading cycles the term "damping" is used. Since loads in this test did not really alternate, but were applied in one direction and varied only in size, the loss of energy is better described by using the term "energy dissipation" rather than damping.
The energy dissipation is defined by:
Energy dissipated = energy input – energy released during unloading
This means that the dissipated energy can be defined as the area between the loading and the unloading curve in a force-displacement graph. For the case at hand this results in an energy dissipation of 46 % for the first loading cycle, and 34 ± 3 % for all other load cycles. The difference between the first and the subsequent loadings can be explained by the fact that during the first loading cycle energy is needed to create the gap. In all other cases the gap was already present, enabling the pile to move with less restraint.

7.6 *Gap formation*

After the first quasi-static loading bubbling of water in the displacement direction was observed during subsequent loading. This indicates closure of a gap. Gap formation was confirmed after the test by draining the excavated area. Gaps were visible around the pile, see Fig. 7.11. The remaining gap at the backside of the pile was measured. This gap had a width of about 30 mm at ground level, and a small weight with a diameter of 5 mm could be lowered into this gap to a depth of 2.5 m below ground level.
An extensive description of the measured test results is given by Bijnagte and Berg, van den, (1989a).

8 Evaluation

8.1 *Evaluation of models and soil parameters*

Three different models were used to calculate the behaviour of a pile due to static and cyclic lateral loading. There are some significant differences between the models,

Fig. 7.11 Picture of the gap behind the pile, after the test.

which are independent of the number of dimensions taken into account. The most important one concerns the modelling of the shearing (slip) and contact (gap formation) mechanisms at the pile-soil interface. Another important aspect responsible for different predictions deals with the rules used to derive the model parameters from the soil investigation tests.

The quasi 3-dimensional (q3-D) finite element model describes the pile-soil interface using a thin cylinder around the pile, in which gap formation and slip are confined. No slip between pile and soil is allowed; in fact a completely rough pile is considered. Gap formation between pile and soil originates as soon as tensile stresses occur.

The elasto-plastic 3-dimensional (3-D) finite element model considered two extreme cases:

- a rough pile with full bonding between pile and soil. Gap formation around the pile is excluded;
- a smooth pile with no tensile or shear bonding between pile and soil. Gap formation originates where tensile stresses occur. Slip between pile and soil takes place as soon as shear stress occurs at the circumference of the pile.

Despite the large differences in modelling the interface behaviour, the difference between the resulting force-displacement curves for the bonded 3-D case and the q3-D case is very small. One would expect the 3-D calculation to be significantly stiffer than the q3-D model since full bonding between soil and pile is present along the whole circumference. The similarity between the two curves can be explained by the different way in which the model parameters are quantified. In the 3-D model for the soft soil layers the shear modulus G is equal to about 15–50 times the undrained shear strength c_u, whereas in the q3-D model a value of 100 times c_u is applied. In both models there is no significant difference between the strength, c_u, of the soft layers.

The 1-dimensional (1-D) model used the p-y curve approach. Derivation of the shear modulus from the ultimate soil strength and the ε_{50}-strain shows values comparable to those used in the full 3-D model.

Another difference is related to the initial state of stress in the soil due to overburden. This is incorporated in the q3-D model and in the 1-D model and neglected in the 3-D model. In both 3-D models the isotropic stress in the soft upper soil layers does not affect the maximum shear stress of the soil since they are modelled with a flow rule according to Tresca (1868). Because most of the plastic deformation takes place in these upper layers it also does not affect the resulting curves. However, if yielding would occur in the deeper sand layers (Mohr-Coulomb model), the 3-D model would predict too soft behaviour. Evaluation of the results showed that local plasticity occurred resulting in a somewhat more flexible behaviour of the pile.

One phenomenon neglected in the q3-D and 1-D models and incorporated in the 3-D model concerns the effect of the horizontal loading on the vertical stress distribution and displacements in the soil. This effect is significant particularly in the soil layers near the pile-top. Since these layers are essential for the lateral pile-soil behaviour, this effect may be important. In the 1-D model the effect is partly incorporated. A wedge type failure mechanism is assumed in defining the p-y curve.

An effect neglected in the 1-D model deals with stress transfer between different soil layers. In the q3-D model only shear stresses can be transmitted from one layer to another whereas in the full 3-D model all stresses can be transferred in all directions.

8.2 *Predicted and measured results*

8.2.1 Static loading

The predicted and the measured load-displacement curves are summarized in Fig. 8.1. Although all effects mentioned before influence the result of the calculation, comparison of model and test results shows that all calculations predicted a too soft or flexible

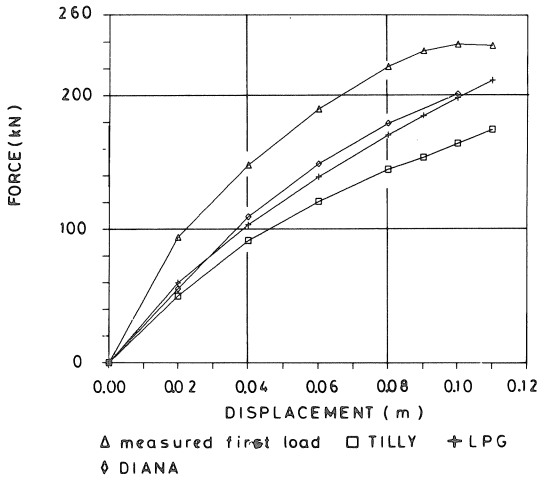

Fig. 8.1 Load-displacement curves: predicted and measured.

behaviour. It can be seen that the actual initial stiffness of the pile-soil system is much higher than the values following from the predicted curves.
This indicates that the design rules used in the application of the different models have to be classified as conservative with respect to a deformation criterion: they overestimate the deformations. This may be considered logical as they implicitly include safety aspects.
A second possible explanation can be found in the rate-dependent stiffness of the soft soil layers. Due to the relatively short-time loading the soil reacts stiffer than under prolonged loading.
All models were used to calculate the bending moment distribution along the pile as a function of the load level. The results show an increasing depth and magnitude of the maximum bending moment at increasing loading. In all cases both depth and magnitude are overestimated with respect to the measured distribution. This is a result of the softer behaviour of the soil in the calculations. The test results show that the sign of the bending moment changes at the top of the deeper sand layers. None of the models predicted this alternation of the sign, indicating that in reality the sandy layers behaved relatively stiffer than adopted in the calculations.

8.2.2 Cyclic loading

The cyclic behaviour of the pile, including degradation and friction between pile and slot-wall, was calculated by the q3-D and 1-D models. The results indicate that the q3-D model is rheologically not yet sufficiently equiped to model the phenomena measured. Part of the difference between the first calculation and the test result is caused by neglecting the presence of adhesion between the pile and the soil. Adding adhesion increases the energy dissipation during a cycle. However, the use of realistic values for

the adhesion still does not result in a good description of the measured behaviour. The 1-D model has empirical tools capable of modelling the measured behaviour. However, it cannot explain the rheology from a physical point of view. Since knowledge about these phenomena is scarce and insufficient and no standard laboratory test is available, the size of the parameters to describe the degradation, backsliding of the gap and the slot-wall friction can not be derived beforehand.
A comparison between the calculations and the test results shows which parameter values give a satisfying agreement for this specific situation, when the parameter values are considered to be the same for all soil layers. For other conditions different values may apply, therefore it is recommended to develop a standard laboratory testing procedure to derive the necessary parameter values.

8.3 *Standard Dutch design method*

In addition to the predictions described in the chapters 4, 5 and 6 a calculation according to the "standard Dutch design rules" was performed. The model applied resembles the 1-D discrete element model described in chapter 4. Differences are that this model is a finite element model, so the elements to model the pile are conventional continuous beam elements. The pile-soil contact is described by springs, together forming a continuous elasto-plastic support. The model is only suited for static calculations, and gap forming is not included.
The coefficient of horizontal subgrade reaction k, the spring stiffness per unit length, was determined using a correlation with the cone resistance. A commonly used relation is: $k \approx 3q_c$. The ultimate force of the springs is calculated according to Brinch Hansen's method (1961). The soft soil layers are considered to react undrained, whereas the sandy layers are supposed to behave drained. The result of the calculation is shown in Fig. 8.2. It shows a far too soft behaviour: the calculated displacements at a given force level far exceed the measured values.

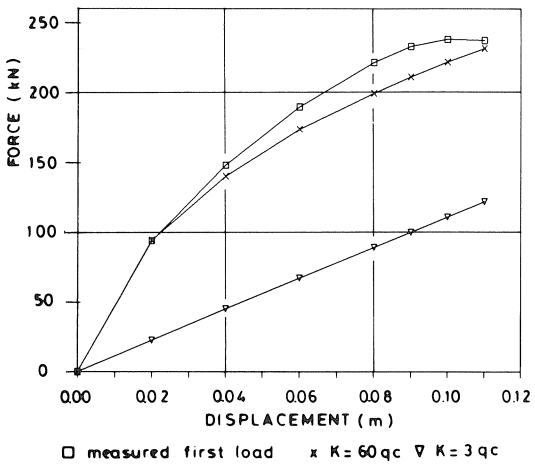

Fig. 8.2 Force-pile top displacement relations "standard Dutch design method" and test.

Comparison of the maximum bending moment as well as the bending moment distribution shows that the calculated values are higher than the measured ones, see Fig. 8.3. Both depth and magnitude are overestimated with respect to the measured distribution due to softer behaviour of the soil in the calculations.

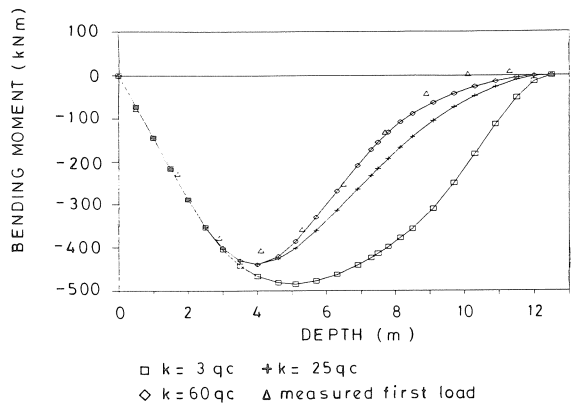

Fig. 8.3 Bending moments in the pile following from a "standard Dutch design method" and measured during the test.

Because of these differences in the force-displacement relations and the force-bending moment distribution, adaptations of the standard design rule have to be proposed for short-duration loading. Additionally a large number of calculations were performed using different values of the coefficient of horizontal subgrade reaction k. The results of these calculations show that for this special case, values of k equal to about 25 to 60 times the cone resistance should be used to tune the results. Fig. 8.2 shows the calculated force-displacement relations for $k = 3q_c$ and $k = 60q_c$. The measured values for the initial loading are also included.

Based on these results it is concluded that for short-duration loads, far higher coefficients of horizontal subgrade reaction should be used than the ones now commmonly applied. This will result in both a better load-displacement prediction and a more realistic bending moment distribution as well. Since the values mentioned here only apply to the studied pile-soil system and loading conditions, a generally valid approach should be developed. This should result in a calculation model in which the influence of the rate of loading is automatically incorporated. A more elaborate description of such a model is given by Bijnagte and v.d. Graaf (1990).

It should be noted that, in addition to the method described before, another design method still popular is the one according to Blum (1932). This method can be applied very easily since the magnitude of the soil reaction stresses does not depend on the strain level (rigid plastic approach). This behaviour does not correspond to real soil behaviour and load-displacement curves due to working loads cannot be obtained. Therefore this method is not considered in this project.

9 Summary and conclusions

In the context of a research project commissioned by the Dutch Ministry of Public Works (Rijkswaterstaat), Delft Geotechnics analysed the behaviour of dolphins subjected to static and cyclic lateral loading both numerically and in a full scale test. The scope of the project was extended to a benchmark prediction by cooperation with two departments of the Civil Engineering Department of Delft University of Technology (Mechanics & Structures Division and Section Geotechnics). Each participant incorporated their own numerical model currently under development.

A 1-dimensional discrete element model (Mechanics & Structures Division), a quasi 3-dimensional elasto-plastic finite element model (Section Geotechnics) and a full 3-dimensional elasto-plastic finite element model (Delft Geotechnics) were used to calculate class "A" predictions for the lateral behaviour of a pile, loaded quasi-statically and cyclically.

The 1-dimensional model consists of rigid elements connected with elasto-plastic springs to model the translational and rotational behaviour of the pile. The pile-soil interaction is modelled with a special element accounting for the elasto-plastic behaviour of the soil, gap formation, degradation of strength due to cyclic loading and backsliding of the gap at unloading.

The most important difference between the 3-dimensional models can be summarized as follows. In the quasi 3-dimensional model the soil consists of a number of horizontal plane strain layers (disks). At the contact area of these disks only shear stresses can be transferred from one layer to another. This implies, that the vertical deformation as well as the increase of the vertical stress due to a horizontal loading is neglected. In the full 3-dimensional model these effects are incorporated.

In addition to the comparison of different models, the effect of different "levels" of soil analysis was included in the project. This resulted in predictions for the load-displacement behaviour based on different soil investigation levels. The first predictions are based on cone penetration testing. In the second phase, extended soil investigations, a boring and laboratory testing, including triaxial and simple shear tests, took place. The final prediction was based on the foregoing results in combination with in situ, pressuremeter, investigation of the stiffness and strength behaviour of the soft soil layers.

The full scale field test was performed on an instrumented hollow steel pile with a diameter of 0.61 m, a wall-thickness of 8.8 mm and a length of 12.5 m. The location of the pile can be characterized as 8 m layered soft soil above medium dense sand, resembling a typical Dutch dolphin location quite well. The load and the displacement of the top of the pile were measured during the test as well as the strains along the pile. The pile was loaded quasi-statically and cyclically. Soil strength degradation, gap formation and other cyclic effects were documented.

Comparison of the predictions with the test results leads to some interesting conclusions. All calculations predict a more flexible behaviour than measured; they overestimate the deflection by a factor between 2 and 3. This phenomenon, referring to ship impact in which a "soft" reaction of a dolphin is favorable, may help to explain un-

expected damage, which often occurs at locations with soft top layers. Due to the true, more stiff, behaviour of the soil, all models overestimate both depth and magnitude of the bending moment in the pile; the differences are in the range of 30 %.
Further conclusions refer to the horizontal stress and deformation patterns in the soil surrounding the pile. These are limited to a rather small zone, so correct characterization of this region is essential for the overall behaviour of the pile. Modelling of the shearing mechanism between pile and soil is very important. The range for the horizontal force at the same pile top displacement resulting from the limit cases, "rough circular pile without the gapping mechanism" and "smooth circular pile" is a factor between 2 and 3, depending on the load level.
Gap formation is restricted to a depth in the range of a few pile diameters and the plastic soil region is limited to a radius of two pile diameters at the surface. Vertical soil stresses and deformations due to horizontal loading occur only in a small zone around the pile top.
Comparison of all models included in the benchmark shows that the 1-dimensional discrete element model performs most effectively for design calculations, for several reasons:
- minimum computing time and simple pre- and post-processing;
- parameter derivation for quasi-static loading for this model is widely accepted;
- cyclic effects and gap formation are included;
- dynamic calculations including pile-ship-interaction are possible within reasonable effort.

Based on the results of this study the parameter derivation methods should be reviewed for horizontal loading of dolphins at Dutch locations rather than improving the calculation models.

10 Acknowledgement

Chapters 4 and 5 have been compiled from reports made by A.J. Grashuis and A.P. Kooijman respectively.

11 Notation

A	area of the pile cross section	[m^2]
c	cohesion	[kN/m^2]
c_u	undrained shear strength	[kN/m^2]
D	pile diameter	[m]
D_{ii}	matrix component, *i-th* row, *i-th* column	[kN/m^2]
E	Young's modulus	[kN/m^2]
f_t	maximum tensile stress	[kN/m^2]
G	shear modulus	[kN/m^2]
PI	Plasticity Index	[weight
%]		
Δu	relative displacement	[m]
V	volume	[m^3]
ΔV	volume change	[m^3]
K_0	lateral stress ratio	[-]
K	bulk modulus	[kN/m^2]
M	bending moment	[kN/m^2]
n	number of loading cycles	[-]
N	normal force	[kN]
N_c	cone factor	[-]
N_0	initial soil strength	[kN/m^2]
N_{ul}	ultimate strength of the soil, after infinite loading cycles	[kN/m^2]
N_{deg}	strength of the degraded soil, in the *i-th* cycle	[kN/m^2]
p	soil resistance per unit pile length	[kN]
p_{lim}	limit pressure	[kN/m^2]
q_c	cone resistance	[kN/m^2]
s	wall thickness	[m]
t	traction	[kN/m^2]
y	displacement	[m]
z	depth below ground level	[m]

α	parameter for the rate of strength reduction	[-]
β	cyclic strength reduction parameter	[-]
γ	unit weight	[kN/m^3]
δ	interface friction angle	[°]
ε	strain	[-]
ν	Poisson's ratio	[-]
ξ	parameter for backsliding of the gap	[-]
ϱ	density	[ton/m^3]

σ	stress	[kN/m^2]
τ	shear stress	[kN/m^2]
ϕ	friction angle	[°]
ψ	dilatancy angle	[°]

subscripts

co	consolidation
d	drained
h	horizontal
i	isotropic
n	normal
s	shear
u	undrained
1	in the pricipal direction 1
2	in the pricipal direction 2
3	in the pricipal direction 3
50	at half the maximum
,n	of element n
ul	ultimate

superscripts

′	effective
-	mean

12 References

API (1984), Recommended practice for planning, designing, and constructing fixed offshore platforms. American Petroleum Institute Washington, D.C.

BAGUELIN, F., J.F. JÉZÉQUEL and D.H. SHIELDS (1978), The Pressuremeter and Foundation Engineering. Trans Tech Publications.

BEGEMANN, H.K.S.PH. (1966), The new apparatus for taking a continuous soil sample, LGM Mededelingen, part X, No. 4, april.

BERG, P. VAN DEN (1991), Numerical model for cone penetration, to be published in Proc. of IACMAG 91 Conf. to be held May 6-10, Cairns, Australia.

BJERRUM, L. and A. LANDVA (1966), Direct simple shear tests on a Norwegian quick clay. Geotechnique 16, No. 1, 1-20.

BLAAUWENDRAAD, J. and A.W.M. KOK (1987), Handicraft in finite elements, Numeta Conf., Swansea,

BLUM, H (1932), Wirtschaftliche Dalbenformen und deren Berechnung. Die Bautechnik 10 No. 5.

BOULON, M. (1989), Basic features of soil structure interface behaviour, Computers and Geotechnics, 7, 115-131.

BOULON, M. and R. NOVA (1990), Modelling of soil structure interface behaviour, a comparison between elastoplastic and rate type laws, Computers and Geotechnics, 9, 21-46.

BRINCH HANSEN, J. (1961), The ultimate resistance of rigid piles against transversal forces. The Danish Geotechnical Institute.

BIJNAGTE, J.L. and P. VAN DEN BERG (1988), "Dolphins numerically II, soil investigations report Level IIIa (in Dutch). Delft Geotechnics report nr. CO-294781/34 (commissioned by the Dutch Ministry of Public Works, Locks and Weirs division).

BIJNAGTE, J.L. and P. VAN DEN BERG (1989a), "Dolphins numerically II, measurement report (in Dutch). Delft Geotechnics report nr. CO-294781/47 (commissioned by the Dutch Ministry of Public Works, Locks and Weirs division).

BIJNAGTE, J.L. and P. VAN DEN BERG (1989b), "Dolphins numerically II, final report (in Dutch). Delft Geotechnics report nr. CO-294781/55 (commissioned by the Dutch Ministry of Public Works, Locks and Weirs division).

BIJNAGTE, J.L. and H. V.D. GRAAF (1990), "Ducbots" Dynamic modelling of dolphins (in Dutch). Delft Geotechnics report nr. CO-294782/27 (commissioned by the Dutch Ministry of Public Works, Locks and Weirs division).

CALLE, E.O.F. (1979), Determination of earth pressures on sheet pile walls from measures of deflections and bending moments. LGM medelingen XX no.4.

COULOMB, C.A. (1776), Essai sur une application des règles de maximis et minimis a quelques problèmes de statique rélatifs a l'architecture, Mémoires de l'Academie Royale des Sciences 7, 343-382.

DNV (1977), Det Norske Veritas: Rules for design, Construction and Inspection of Fixed Offshore Structures.

GRASHUIS, A.J. (1988), The implementation of the hygade element including cyclic degradation in TILLY, Master Thesis Delft University of Technology (in Dutch).

GRASHUIS, A.J. (1989), Dolphin Research II, Predictions TILLY-Hygade, Appendix of Delft Geotechnics report nr. CO-294781/55 (in Dutch).

GRASHUIS, A.J., H.A. DIETERMAN and N.F. ZORN (1991), Calculations of cyclic response of laterally loaded piles, accepted for publication by Computers and Geotechnics.

HEAD, K.H. (1984), Manual of Soil Laboratory Testing, Volume 1: Soil Classification and Compaction tests. Pentech Press.

HEAD, K.H. (1988), Manual of Soil Laboratory Testing, Volume 2: Permeability, Shear Strength and Compressibility Tests. Pentech Press.

HEAD, K.H. (1986), Manual of Soil Laboratory Testing, Volume 3: Effective Stress Tests Pentech Press.

HEINSBROEK, A.G.T.H. and J. BLAAUWENDRAAD (1989), Reinforced concrete beams under shock loading; linear and non-linear respons, Heron, vol. 34.

L'HERMINIER, R. (1953), Le pénétromètre et les fondations superficielles, Ann. ITBTP, 1953 (63/64), 377-386.
KOOIJMAN, A.P and P.A. VERMEER (1990), Elastoplastic analysis of laterally loaded piles, Proc. 2nd Int. Conf. Num. Meth. Geomech., Innsbruck, 1033-1042.
KOOIJMAN A.P.(1988), Class 'A' predictions of a laterally loaded single pile foundation Delft, Delft University of Technology (in Dutch).
KOOIJMAN A.P.(1989a), Quasi three-dimensional model for laterally loaded piles, Proc. 8th Int. Conf. Offsh. Mech. Arctic. Engng., The Hague.
KOOIJMAN A.P.(1989b), Numerical Model for laterally loaded piles and pile groups, Doctor's Thesis Delft University of Technology.
LAMBE, T.W. and R.V. WHITMAN (1969), Soil Mechanics, SI Version. John Wiley & Sons, New York.
MATLOCK, H. (1970), Correlations for design of laterally loaded piles in soft clay, 2nd Offsh. Techn. Conf., Texas, OTC 1204.
RANKINE, W.J.M. (1857), On the stability of loose earth, Phil. Trans. Roy. Soc., London, 147, Part 1, 9-27.
RUITER, J. DE (1982), The static cone penetration test - state of the art, ESOPT II, 2, 389-405, Amsterdam.
SULLIVAN, W.R., L.C. REESE and C.W. FENSKE (1980), Unified method for analysis of laterally loaded piles in clay, In: Numerical Methods in Offshore Piling, The Institution of Civil Engineers, Londen, 135-146.
TERZAGHI, K and R.B. PECK (1967), Soil Mechanics in Engineering Practice, second edition, John Wiley and Sons.
TRESCA, H. (1868), Mémoire sur l'écoulement des corps solides, Mém. pres. par div. Savants 18, 733-799.
VERMEER, P.A. and R. DE BORST (1984), Non-associated plasticity for soils, concrete and rock, Herin, Volume 29, No. 3.
VERRUIJT, A. and A.P. KOOIJMAN (1989), Laterally loaded piles in a layered elastic medium, Geotechnique 39 No. 1, 39-46.
VESIC, A.S. (1972), Expansion of cavities in infinite soil mass, Int. J. Soil Mech. Found. Div. ASCE, 98, 265-290.